



Review

Magnesium research and applications: Past, present and future

Jianyue Zhang^{a,1}, Jiashi Miao^{a,1}, Nagasivamuni Balasubramani^a, Dae Hyun Cho^a,
Thomas Avey^a, Chia-Yu Chang^a, Alan A. Luo^{a,b,*}^aDepartment of Materials Science and Engineering, The Ohio State University, Columbus, OH 43210, USA^bDepartment of Integrated Systems Engineering, The Ohio State University, Columbus, OH 43210, USA

Received 25 October 2023; received in revised form 15 November 2023; accepted 17 November 2023

Available online 5 December 2023

Abstract

As the lightest structural metal and one of the most abundant metallic elements on earth, magnesium (Mg) has been used as an “industrial metal” for lightweighting in the transportation and electronics industries, in addition to other traditional applications in aluminum alloying, steel desulfurization and protective anodes. In recent years, research has shown significant potential for Mg to become a “technology metal” in a variety of new applications from energy storage/battery to biomedical products. However, global Mg production has shown steady but moderate growth in the last three decades. Mg applications as an industry metal are still limited due to some sustainability concerns of primary Mg production, as well as a number of technical issues related to the structural and corrosion performance of commercial Mg alloys. New Mg applications as an industrial or technology metal face tremendous technical challenges, which have been reflected in the intensified global research efforts in the last twenty years. This paper will review some past and present applications, and discuss future opportunities and challenges for Mg research and applications for the global Mg community.

© 2023 Chongqing University. Publishing services provided by Elsevier B.V. on behalf of KeAi Communications Co. Ltd.

This is an open access article under the CC BY-NC-ND license (<http://creativecommons.org/licenses/by-nc-nd/4.0/>)

Peer review under responsibility of Chongqing University

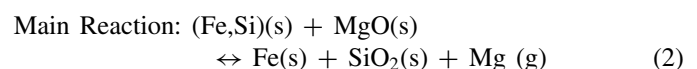
Keywords: Magnesium alloys; Structural applications; Lightweighting; Biomedical applications; Energy applications.

1. Introduction

Magnesium (Mg) is the fifth most abundant metallic element in earth's crust (about 2%) and the third most abundant in seawater (about 0.13%). According to the United States Geological Survey [1], resources from which Mg may be recovered range from large to virtually unlimited and are globally widespread. Resources of dolomite, serpentine, and Mg-bearing evaporite minerals are enormous. Mg-bearing brines are estimated to constitute a resource in the billions of tons, and magnesium could be recovered from seawater along world coastlines.

The Mg metal was first produced in England by Sir Humphry Davy in 1808 using electrolysis of a mixture of magnesia and HgO. Table 1 shows that the world Mg pro-

duction has reached a total production of over one million metric tons in 8 countries, with China leading in producing about 90% of the world supply. The production process used in China is a silicothermic reduction process called Pidgeon process, originally developed by a Canadian chemist Lloyd Pidgeon. This is a batch process in which dolomite (Ca,Mg)CO₃ is finely powdered and calcined, as shown in Reaction (1), mixed with ferrosilicon (Fe,Si) and briquetted, and then charged in retorts made of nickel-chrome-steel alloy. The calcium oxide present in the reaction zone scavenges the silica formed, Reaction (2), releasing heat and consuming one of the products, thus helping push the main reaction (2) to produce the Mg vapor.



* Corresponding author.

E-mail address: luo.445@osu.edu (A.A. Luo).¹ These authors contributed equally: Jianyue Zhang, Jiashi Miao.

Table 1
Mg metal production in 2021 and 2022 (unit: thousand metric tons) [1].

Year	Brazil	China	Israel	Kazakhstan	Russia	Turkey	Ukraine	USA	Total*
2021	20	930 ^a	18	16	58 ^a	13	10	W**	1070
2022 ^a	20	950	22	15	50	13	2	W	1080

^a Estimated.

* World total excluding U.S. production.

** Withheld to avoid disclosing company proprietary data.

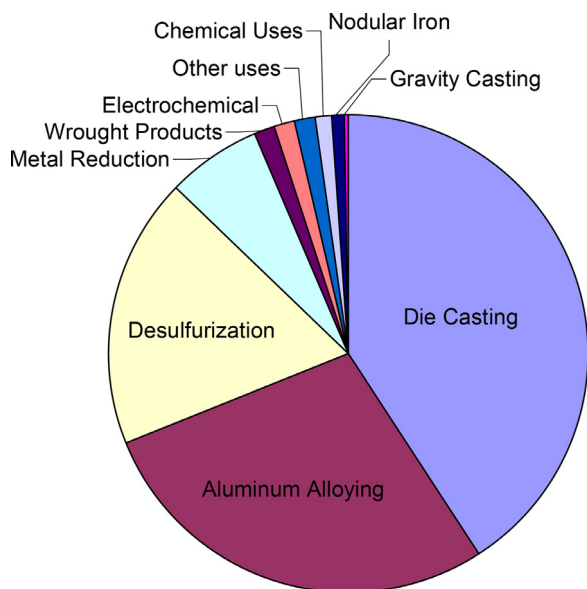


Fig. 1. Industrial applications of magnesium and magnesium alloys.

The hot reaction zone portion of the retort is either gas-fired, coal-fired, or electrically heated in a furnace, while the condensing section equipped with removable baffles extends from the furnace and is water-cooled. Due to distillation, very high purity Mg crowns are produced, which are then refined and cast into ingots. However, this process is very energy-intensive and inherently releases significant amounts of CO₂, averaged at about 21.8 kg CO_{2eq}/kg Mg [2].

With a density of 1.74 g/cm³, Mg is the lightest of all commonly used structural materials, lighter than aluminum but similar to carbon fiber reinforced polymers (CFRP) or glass fiber reinforced polymers (GFRP). Mg has found many industrial applications, as shown in Fig. 1, such as die casting, aluminum alloying, steel desulfurization, metal reduction, etc. In recent years, research has shown significant potential for Mg to become a “technology metal” in a variety of new applications from energy storage/battery to biomedical products. Fig. 2 shows that the world demand for Mg has seen steady but moderate growth in the last 20 years [2] Specifically, the automotive share of Mg applications has not grown as many predicted, in some cases, losing to other materials.

In the last decades, the global energy and transportation industries are facing increasingly pressing sustainability challenges. Fossil fuels, including coal, oil, and natural gas, have been powering economies for over 150 years, and currently supply more than 80% of the world’s energy. Major

transportation original equipment manufacturers (OEMs) and governments around the world have made commitments to carbon-zero/neutral by 2035–2050. Therefore, the embodied energy of a material, i.e., the energy of the fossil fuel consumed to produce 1 kg of the material, has become a critical criterion for its selection in industrial applications. As shown in Fig. 3, despite the low-density advantage of Mg, it has a very high embodied energy (second only to titanium), due to the high energy consumption and inherent CO₂ emissions of the Pidgeon process. Thus, there is an increasing concern for OEMs to select/increase Mg’s use for lightweight applications.

Going forward, in order to map out the future for Mg, we must understand where it is now compared with other metals in world production and applications. Fig. 4 shows the world metal production in 2021 [5] with iron/steel dominating and Al leading the “industrial metal” production. With an annual output about 1 million tonnes, Mg is a very small industrial metal, which is about 1.5% of Al production. On the other hand, Mg is not considered a “technology and precious metal” (such as Li) where it is used in high-valued applications, despite low tonnage in many cases.

The current drive for clean energy and environmental sustainability has posed significant challenges to Mg, both as an “industrial metal” for its traditional applications and a “technology metal” for future applications. This paper will discuss the future opportunities and challenges for Mg research and applications for the global Mg community responding to these unprecedented challenges. It will also provide an overview of recent Mg alloy development and process innovations at The Ohio State University in collaboration with its industrial partners, for structural and biomedical applications.

2. Magnesium applications

2.1. Historical and present applications as an industrial metal

While magnesium can be used for alloying and chemical applications (Fig. 1), this section is more concerned with lightweight applications in automotive, aerospace, electronics and other industries. The first automotive application of magnesium can go back to more than 100 years ago when Dow Chemical built their racing engine pistons and won the Indy 500 in 1921 (Fig. 5a). This was followed by the famous engine block in the Volkswagen Beetle in mid 1930’s. The first use of Mg in airplanes was probably Mg sheet in Focke-Wulf 200C-3 Condor as early as 1935 [6]. During World War II, the U.S. and British military aircraft used sand cast Mg wheels. In 1950’s B-36 Bomber had extensive use of 12,200 lbs Mg sheet; 1500 lbs Mg forgings; and 660 lbs. of Mg castings (Fig. 5b) [6]. Since then, Mg applications as a lightweight material has been up and down during the last century.

Over the last few decades, extensive research and development efforts by the automotive manufacturers, Mg and component suppliers have resulted in many applications of

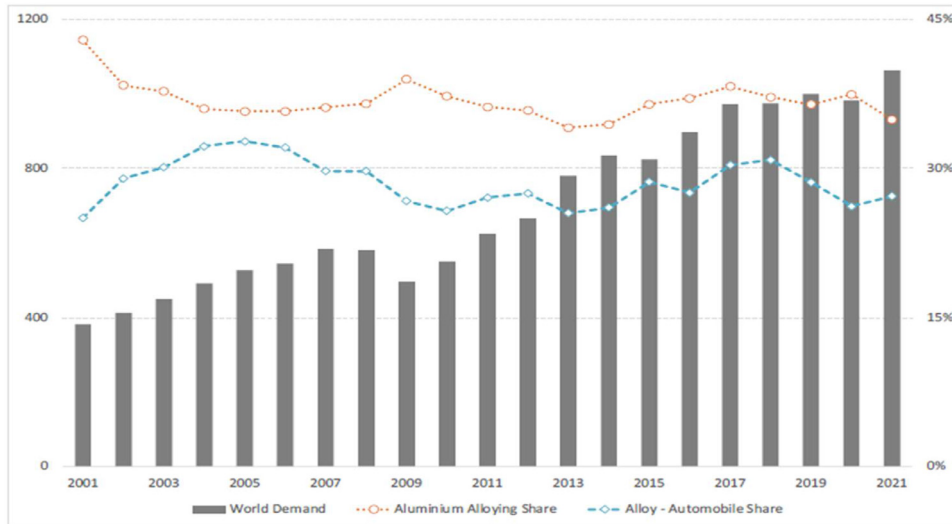


Fig. 2. Global magnesium supply and demand in the last 20 years [3].

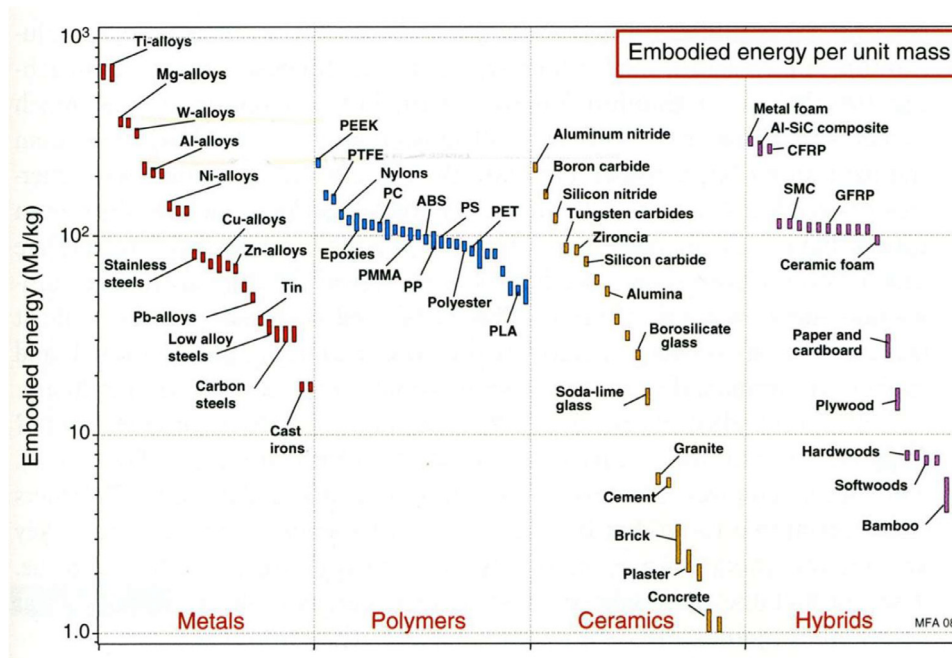


Fig. 3. Embodies energies of materials per unit mass [4].

Mg alloys in automotive interior, chassis, body and power-train systems [7] A recent review article published in this journals provided a good summary of automotive Mg applications around the world [8]. Despite the large number of applications which have been explored or used with Mg at different times, it remains a relatively small percentage of the materials in a typical vehicle as shown in Fig. 6, which was 16 lbs (7.3 kg and ~ 0.4% of total vehicle weight) in 2022 and projected to grow to 18 lbs in 2026. There are many reasons for the lack of use including the high cost and limited supply based of Mg (at least in North America and Europe), low formability limiting its use in sheet metal components, low corrosion resistance, and limited overall design and man-

ufacturing experience with the material compared with steel or aluminum alloys.

Although Mg has been attractive to aerospace and aviation industries with numerous historical applications (mostly in military aircraft), there are some drawbacks, such as flammability, ignition temperature, and corrosion resistance, that limited its use in modern commercial aviation. In fact, Mg had been banned from aircraft seat application by the U.S. Federal Aviation Administration (FAA) [10] until 2015 when the Society of Automotive Engineers (SAE) issued a new performance standard AS8049C that permits the use of Mg alloys in aircraft seat components [11]. However, the current International Air Transport Association (IATA) regulations



Fig. 4. World metal production in 2021 [5].

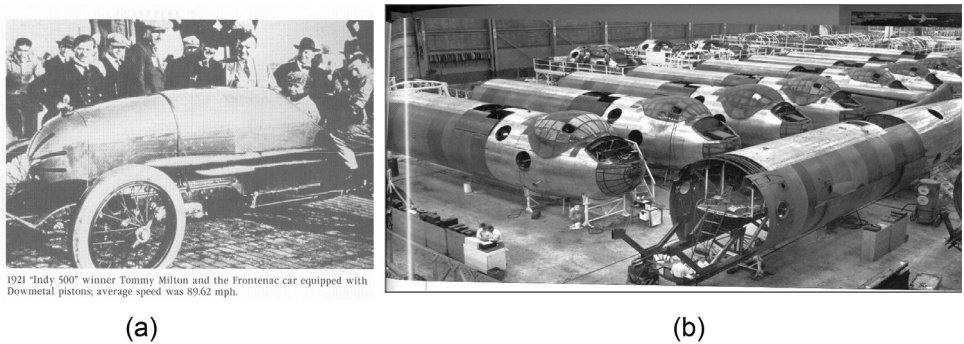


Fig. 5. (a) First Mg automotive application - Dowmetal (magnesium) pistons in 1921. (b) B36 assembly line in 1950's with extensive use of Mg castings, forgings and sheet components.

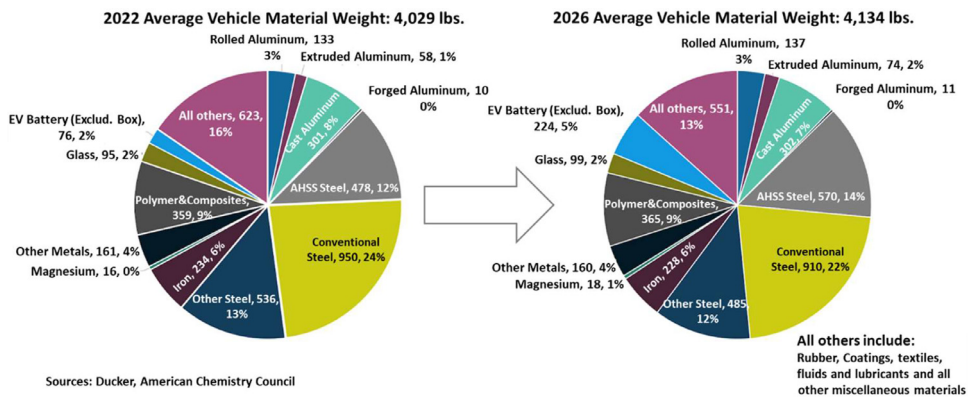


Fig. 6. Average material content evolution from 2022 to 2026 [9].

still restrict the use of Mg to non-structural applications due to potential problems with corrosion. Thus, Mg castings are used in some engine auxiliary components and transmission housing. The improved mechanical properties and corrosion resistance of new Mg alloys developed in recent years could lead to more Mg aerospace applications in the future. A recent global aerospace magnesium alloys market study [12] sug-

gested that this market was valued at US\$ 201.7 million in 2022 and was projected to reach US\$ 325.6 million by 2029, at a compound annual growth rate (CAGR) of 7.1% during the forecast period.

As an industrial metal, Mg has been successful in replacing plastics and polymers as casing material for electronic and consumer products where its electromagnetic shielding char-

acteristics, heat dissipation capacity and machinability can extend the lifetime of these high-volume products. Similarly, Mg is replacing steel and Al in many applications such as electronic/consumer products, hand tools, safety protection (e.g., helmet) and construction equipment (e.g., formwork) where its low density is important consideration.

2.2. Emerging applications as a technology metal

In the last decade, research has shown significant potential for Mg to become a “technology metal” in a variety of new applications from biomedical products to energy storage/battery.

Mg has gained significant attention in recent years as a potential material for biodegradable implants [13,14]. The motivation for choosing biodegradable implants over non-degradable metallic implants like titanium (Ti) alloys, cobalt-chromium (Co-Cr) alloys, and stainless steel stems from issues such as stress shielding, metal ion release, and secondary infections [15]. Additionally, the long healing time and non-degradability of non-biodegradable implants often require a secondary surgery for removal or replacement after healing [16].

A comprehensive report by Frank Witte titled “History of Biodegradable Magnesium Implants” chronicles the various attempts and limitations in early research on biodegradable Mg alloy applications up until the 1980s [17]. Notable examples of cardiovascular and musculoskeletal applications of biodegradable Mg alloys and the limitations of their clinical use are mentioned in the report. Commercially available clinical applications began with the introduction of the absorbable magnesium stent, DREAMS 2G, by Biotronix in 2005. Biotronix conducted feasibility and stability evaluations by implanting these stents into 123 patients with coronary artery disease, using one stent per patient. Clinical results demonstrated complete degradation after 9 months post-implantation, and stability was confirmed through follow-up examinations after 12 months, leading to CE (Conformite Europeene) certification. In 2016, it became the first biodegradable Mg alloy stent to be sold in Europe under the brand name Magmaris® [18,19]. Other commercial products in the form of screws include MAGNEZIX® (Syntellix AG, Germany) and RESOMET/K-MET™ (U&I Corporation, Korea) [20]. In 2013, Magnezix® became the first approved and CE-certified biodegradable screw manufactured using the powder metallurgy (PM) route. This Mg screw, made of uncoated Mg-Y-RE-Zr alloy, received approval for bone fixation and fragments [21,22]. In 2015, another Mg alloy (Mg-Ca-Zn alloy) screw, RESOMET/K-MET (U&I, Korea), was approved in Korea for successful knuckle fixation with no complications [23]. In May 2020, Dongguan Eontec Co., Ltd. China obtained a CE certificate for a high-purity magnesium screw. Furthermore, various studies have reported that the released Mg ions during the degradation process can promote the proliferation of osteoblasts and enhance bone formation [24–27].

Although lithium-ion batteries currently power our cell phones, laptops and electric vehicles, New battery chemistries

are constantly sought out to offer increased energy, greater stability and longer lifetimes. One potential promising element that could form the basis of new batteries is Mg, and Mg-ion batteries could one day play a major role in powering our future, due to its lower cost and a more abundant and robust supply chain. In principle, Mg-ion batteries function very similarly to current Li-ion batteries. Mg ions are shuttled between a negative anode (Mg metal) and a positive cathode, made of a metal-oxide material, which allows electrons to zip around an external circuit and become a battery (Fig. 7).

However, the limited development in electrolytes and cathodes has prevented their commercialization to date. The schematic in Fig. 8 shows an overview of the available Mg battery electrolyte choices in each category, and the advantages/disadvantages associated with each of them. In each category, potential pathways for developing electrolytes with state-of-the-art performance metrics are highlighted.

Magnesium hydride (MgH₂) has a notable attribute of higher gravimetry capacity of 7.2% (mass) and lower cost compared to certain high value elements such as Li [29]. Several investigations showed that Mg based alloys have higher potential due to its light weight and the capacity to store higher volumetric density of hydrogen. However, the hydrogenation/dehydrogenation cycle was sluggish and requires higher operating temperatures (>300 °C). The thermodynamics of the hydriding reaction can be explained using pressure, concentration, and temperature (PCT) diagram shown in Fig. 9(a) [30]. At a given pressure, higher temperature is needed (T₄ to T₁) to achieve a better kinetics of the hydrogenation process. The β -MgH₂ has a reaction enthalpy of -74.5 KJ/mol H₂ (stable hydride region), which requires a temperature of 278 °C for dehydrogenation. The Van't Hoff plot shows the relation between the pressure and temperature, where the slope of the linear fit indicates the enthalpy (ΔH) of the hydrogenation reactions. Reducing the ΔH values to 20–50 KJ/mol H₂ would be the ideal for mobility applications [29].

As discussed in the above section, the magnesium industry is at a crossroads, 1) facing severe competition, as an “industrial metal”, from major industrial materials such as steel, aluminum, plastics and carbon-fiber reinforced composites; and 2) many technical challenges to emerge as a “technology metal” for biomedical and energy applications. The following sections summarize the strategies and recent research for magnesium to grow as an industrial metal and a technology metal in the future.

2.3. Life cycle assessment and sustainability

In 2013, the International Magnesium Association (IMA) published a study “Life Cycle Assessment (LCA) of Magnesium Components in Vehicle Construction” which was written by the Institute of Vehicle Concepts of the German Aerospace Centre (DLR) [32]. The study analyzed the entire life cycle of Mg components for transportation applications, including the production of primary Mg, alloying, component production, use phase and the end-of-life of Mg components. The focus

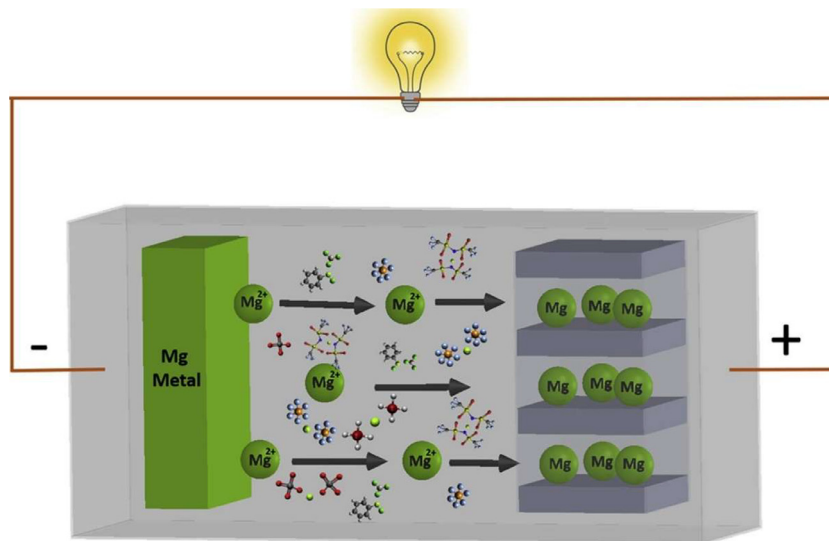


Fig. 7. A schematic illustration of Mg-ion battery [28].

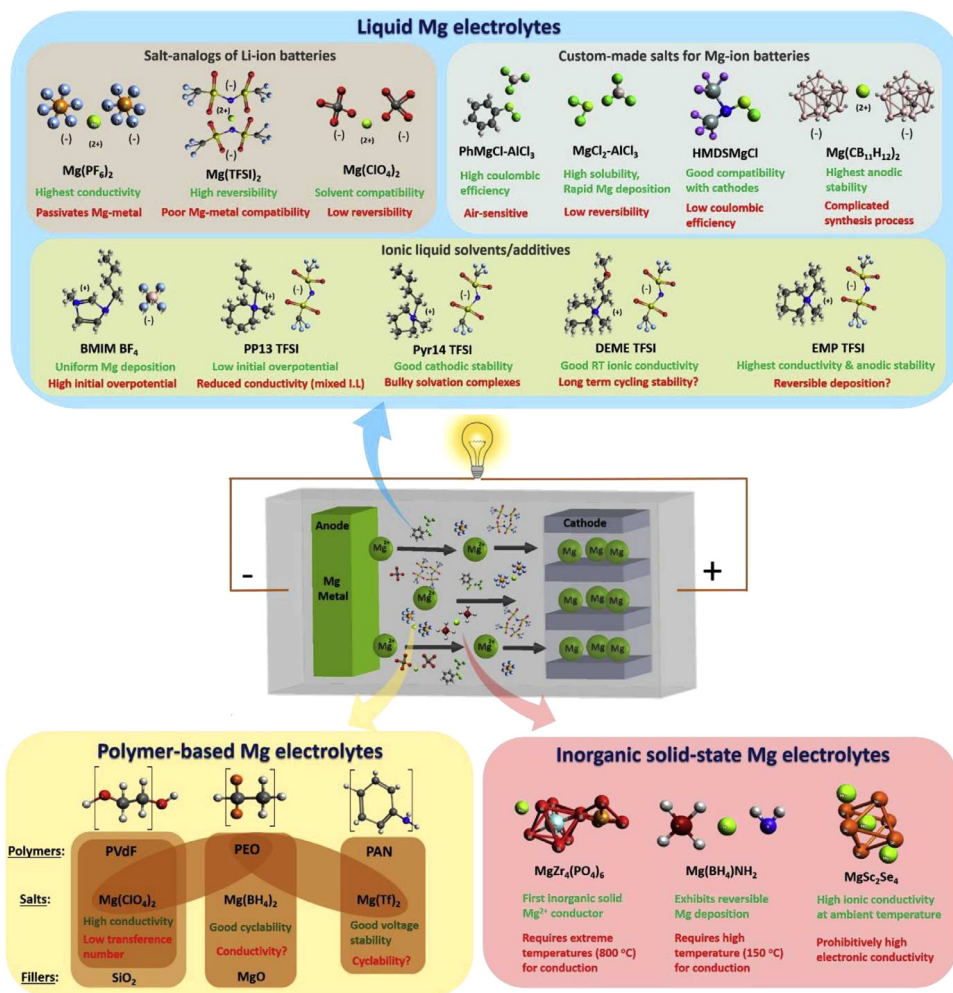


Fig. 8. Schematic illustrating the available choices of electrolyte-salts and additives for a Mg-metal battery, along with their respective advantages (text in green) and their disadvantages (text in red). The shaded regions in ‘Polymer-based Mg electrolytes’ indicate the combinations that have been successfully demonstrated [28].

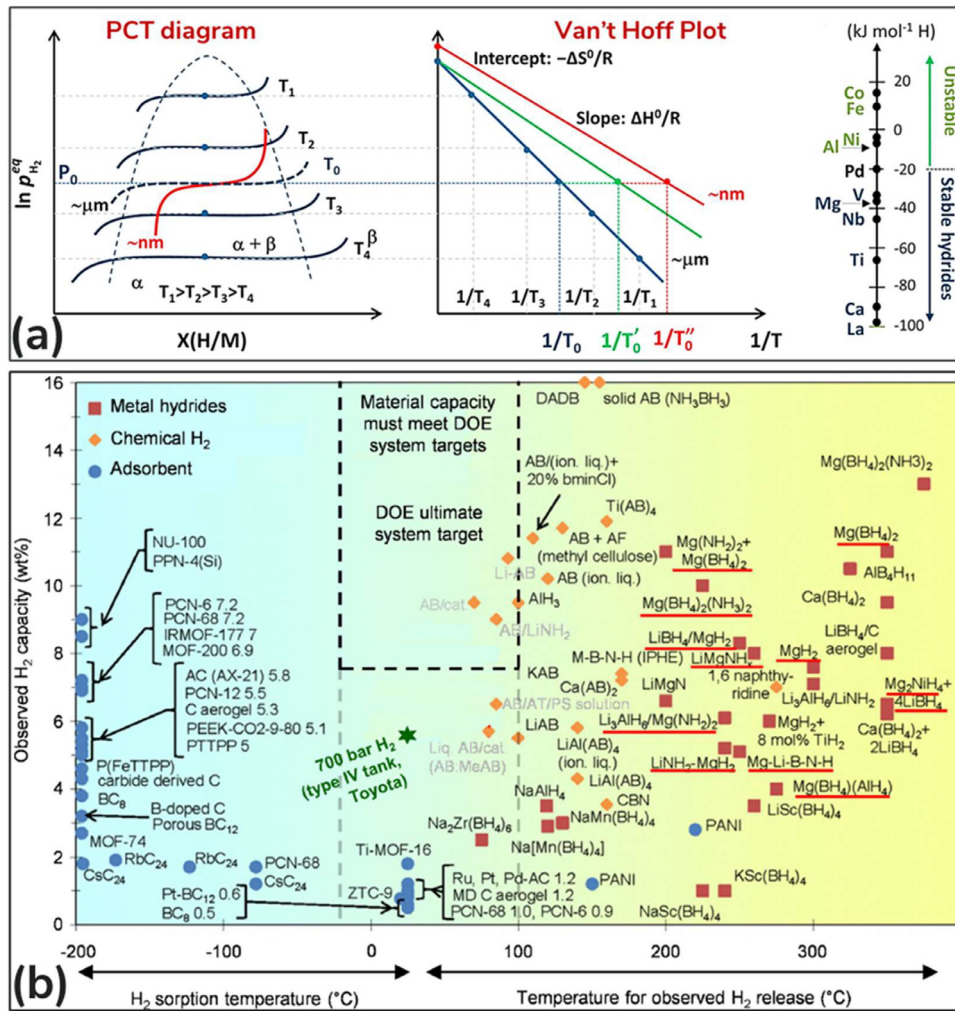


Fig. 9. (a) PCT diagram and Van't Hoff plot explaining the enthalpy change (ΔH) associated with metal hydrides [30]. (b) Solid-state hydrogen storage materials focusing on metal hydrides, chemical and adsorbents. The asterisk mark refers to the type-IV compressed tanks used in Toyota fuel cell car and bus (700 bar compressed gas, two tanks) [31].

of the study was the use of Mg in passenger vehicles, with additional examples of Mg use as aircraft component evaluated. In 2011, the Pidgeon process in Mg production yielded a weighted greenhouse gas emission of 25.8 kg CO_{2eq}/kg Mg [32]. Since Mg production and especially the Pidgeon process in China has seen continuous improvements, an update of the LCA study, based on the data provided by China Magnesium Association (CMA) on Pidgeon process in China, was published in 2020 [2]. Fig. 10 shows the total greenhouse gas emissions of the Pidgeon process. The calculation included all upstream processes like FeSi or fuel gas production, and the results are shown for each step of the Pidgeon process and for the scenarios which reflect the use of four different fuel gases. For better transparency, the impact of the production of dolomite, FeSi and CaF_2 are shown separately. Despite the continuous improvements in process efficiency, the greenhouse emissions of the Pidgeon process remain high, averaged at about 21.8 kg CO_{2eq}/kg Mg [2], which is signif-

icantly higher than 4 kg CO_{2eq}/kg Al in hydropower-based aluminum production [33]

On the other hand, the use of secondary materials is a critical factor in their LCA and sustainability. Although there are established end-of-life (EOL) recycling loops for major industrial metals such as steel and aluminum, such a loop for Mg recycling has not been established due to the limited Mg content in EOL products such as scraped vehicles. However, Mg scrap generated during manufacturing such as die casting is recycled in-house (on manufacturing sites) or shipped to dedicated recycling plants. Fig. 11 shows that the two Mg recycling plants in Europe have significantly lower emission, about 0.4 kg CO_{2eq}/kg Mg, than primary Mg production.

Presently, Mg is losing its favor as a lightweight material to many automotive and aerospace original equipment manufacturers (OEMs) due to its sustainability and supply base concerns. For Mg to become a major industrial metal or grow as a technology metal, low-carbon production process

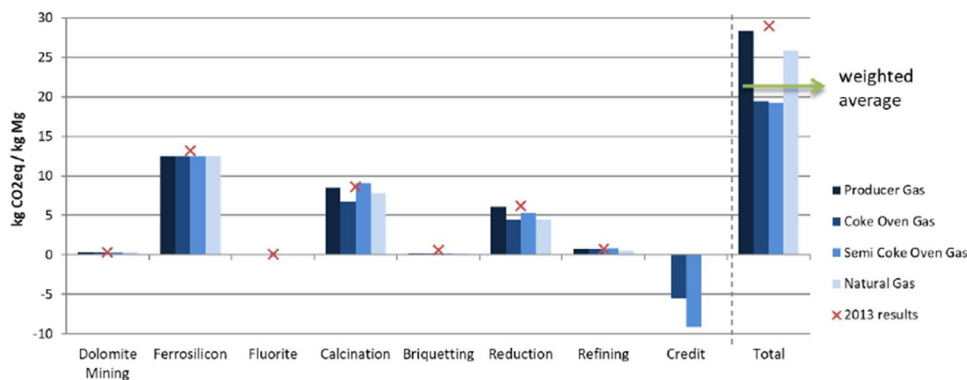


Fig. 10. Greenhouse gas emissions of Pidgeon process [2].

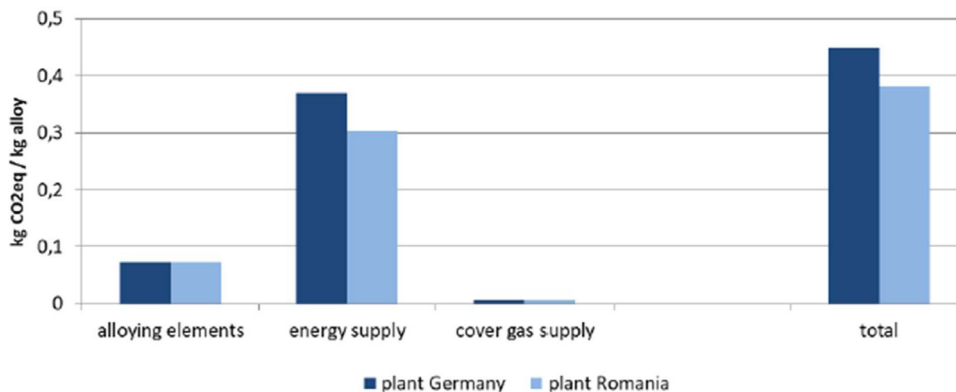


Fig. 11. Greenhouse gas emissions from the recycling of new magnesium scrap [2].

is needed. It is suggested to improve the sustainability of Mg in the future:

- 1) Traditional Pidgeon process production needs to be dramatically improved or gradually phased out due to its inherent CO₂ emissions.
- 2) More production of Mg is needed using electrolytical or non-carbon thermal reduction processes.
- 3) Increased recycling especially EOL Mg to produce secondary alloys to achieve material circularity.
- 4) Mg alloy design and development for recycling and sustainability (e.g., with more tolerance of impurity due to EOL recycling).

3. Recent advances in magnesium alloy development

3.1. Cast alloy development

The conventional cast Mg alloys, including Mg-Al-Zn (AZ), Mg-Al-Mn (AM) and Mg-Al-RE (AE) [34,35], are widely used due to the excellent castability and low cost, but lack strength compared to cast Al alloys. Additionally, it is difficult to achieve significant aging response in these alloys since the number density of main precipitate phase (Mg₁₇Al₁₂) is relatively low and not effective in impeding dislocation gliding. Over the last couple of decades, many new Mg alloys containing Ca, Sn, Si and various RE ele-

ments have been developed to offer improved strength for high pressure die casting and other casting processes. Table 2 summarizes the nominal compositions and tensile properties of some of these new alloys in comparison with commercial alloys (AZ91D, AM50 and AE42). The following points highlights potential areas for future research.

- 1) For high pressure die casting (HPDC) applications, Mg-Al-Ca alloys show significantly improved tensile yield strength, elongation, and creep resistance. Mg-Ce-Mn alloys offer excellent elongation and reasonable strength. Mg-Al-Sn alloys provide potential for age-hardening. These alloys can be further optimized for castability and corrosion resistance.
- 2) For sand casting applications, NZ30K alloy provides excellent tensile strength and ductility after heat treatments (T6 and T7). This alloy has seen some commercial applications.
- 3) Mg-Zn-Ca based alloys have shown outstanding mechanical properties and corrosion resistance in squeeze casting conditions, promising both structural and biomedical applications.
- 4) The addition of Gd to Mg can lead to great precipitation potential, thus, Mg-8Gd-3Y-0.5Zr² (GW83K) alloy reaches outstanding yield strength (236 MPa) and ultimate ten-

² all compositions are in weight percentage unless otherwise stated.

Table 2
Nominal compositions and tensile properties of cast magnesium alloys.

Alloy	Manufacturing process	YS (MPa)	UTS (MPa)	Elongation (%)	Ref
AE42 (Mg-4Al-2RE)	high pressure die casting	137	226	11	[35]
AM50(Mg-5Al-0.5Mn)	high pressure die casting	116	205	9	
AX51(Mg-5Al-1Ca)	high pressure die casting	128	192	6.7	
AX52(Mg-5Al-2Ca)	high pressure die casting	161	228	13	
AX53(Mg-5Al-3Ca)	high pressure die casting	186	250	9	
AZ91D(Mg-9Al-1Zn-0.3Mn)-F	high pressure die casting	160	250	6	
Mg-4Ce-0.5Mn	high pressure die casting	~137	~150	~1.5%	[36]
Mg-4Ce-1Al-0.5Mn	high pressure die casting	~135	~177	~2.8%	
Mg-4Ce-2Al-0.5Mn	high pressure die casting	~130	~239	~12.6%	
Mg-4Ce-3Al-0.5Mn	high pressure die casting	~145	~252	~14.2%	
Mg-4Ce-4Al-0.5Mn	high pressure die casting	~155	~262	~12.9%	
Mg-4Ce-5Al-0.5Mn	high pressure die casting	~152	~265	~12.5%	
Mg-4Ce-6Al-0.5Mn	high pressure die casting	~150	~258	~9.5%	
AZ91D(Mg-9Al-1Zn-0.3Mn)-F	high pressure die casting	160	230	3	[37]
AM60B(Mg-6Al-0.3Zn)-F	high pressure die casting	130	220	8	
AT72(Mg-7Al-2Sn)-F	high pressure die casting	142.9	214.9	6.4	[38]
AT72(Mg-7Al-2Sn)-T4	high pressure die casting	87.9	249.0	11.8	
AT72(Mg-7Al-2Sn)-T6	high pressure die casting	118.0	227.1	4.5	
ATS(Mg-7Al-2Sn-0.4Si)-F	high pressure die casting	156.8 ± 4.5	232.2 ± 4.8	4.2 ± 0.4	[39]
ATS(Mg-7Al-2Sn-0.4Si)-T6	high pressure die casting	154.0 ± 2.9	252.7 ± 15.4	4.9 ± 1.1	
AZ91D(Mg-9Al-1Zn-0.3Mn)-T6	sand casting	131±4.2	243±4.6	4.2±0.6	[40]
NZ30K(Mg-3RE-0.3Zn-0.5Zr)-F	sand casting	92		9.5%	[41]
NZ30K(Mg-3RE-0.3Zn-0.5Zr)-T4	sand casting	88		15.6%	
NZ30K(Mg-3RE-0.3Zn-0.5Zr)-T6	sand casting	165		6.9%	
NZ30K(Mg-3RE-0.3Zn-0.5Zr)-T7	sand casting	138		12.7%	
Mg-4Zn-0.5Ca	squeeze casting	115 ± 6	202 ± 8	15 ± 2	[42]
Mg-4Zn-0.5Ca-0.4Mn	squeeze casting	153 ± 5	234 ± 6	17 ± 2	
Mg-4Zn-0.5Ca-0.8Mn	squeeze casting	201 ± 6	280 ± 5	22 ± 2	
GW83K(Mg-9Gd-3Y-0.4Zr)-T4	semi-continuous casting	132 ± 3	245 ± 4	16.2 ± 2.4	[43]
GW83K(Mg-9Gd-3Y-0.4Zr)-T6	semi-continuous casting	236 ± 5	350 ± 7	3.1 ± 0.5	

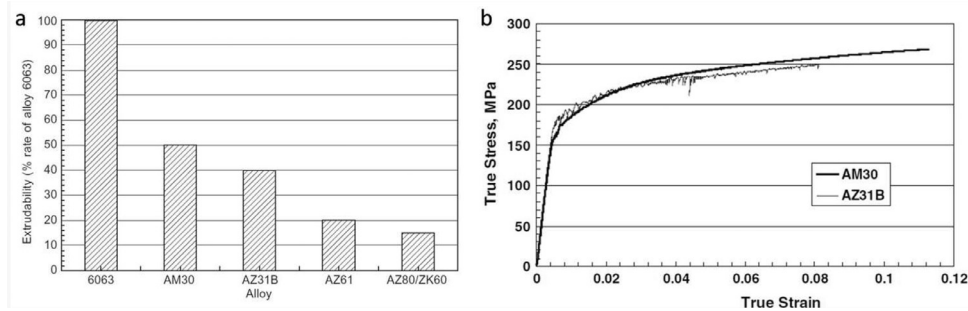


Fig. 12. (a) Comparison of extrudability among AM30 alloy, other extruded magnesium alloys and AA6063 alloy, (b) comparison of tensile properties between AM30 alloy and AZ31 alloy [45].

sile strength (350 MPa) after T6 treatment. The outstanding tensile properties result from concurrent strengthening of precipitation and long period stacking ordered (LPSO) phases.

3.2. Extrusion alloy development

While high pressure die casting is the dominant process for current Mg structural applications, wrought Mg alloys are receiving increasing attention, to achieve improved mechanical and physical properties, crash performance and corrosion resistance. Commercially available wrought Mg alloys,

such as Mg-6Al-1Zn (AZ61) and Mg-6Zn-0.5Zr (ZK60), exhibit yield strengths comparable to those of AA6063 alloy [44]. However, in comparison to Al extrusion alloys such as AA6063, those Mg alloys exhibit significantly lower extrudability as shown in Fig. 10(a), thus requiring extrusion at lower speeds and within a narrower range of extrusion temperatures. The limited extrudability of wrought Mg alloys results in lower production efficiency and higher costs compared to Al extrusion alloys. By reducing the Al content, AZ31 exhibits an improved extrudability as compared with AZ61 and ZK60 alloy. But its extrudability is still much lower than AA6063 alloy as shown in Fig. 12(a). AM30 (Mg-

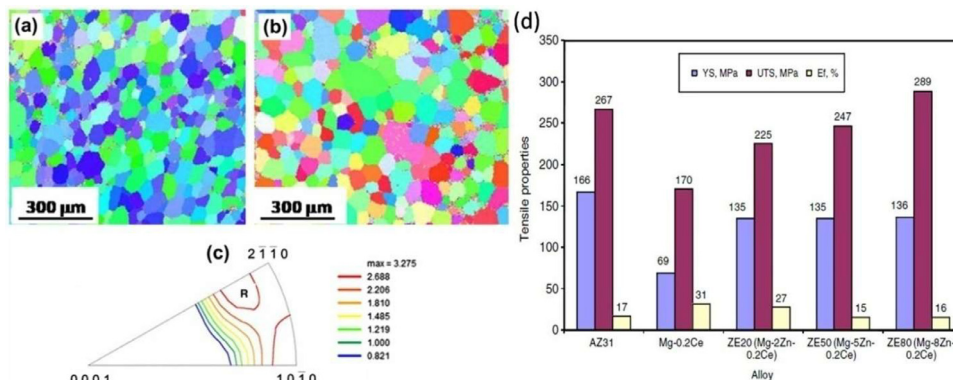


Fig. 13. (a) EBSD IPF map of transverse direction, (b) EBSD IPF map of longitudinal direction, (c) texture IPF of transverse direction of ZE20 alloy extruded at $0.1 \text{ m}\cdot\text{s}^{-1}$, and (d) the comparison of tensile properties of ZE alloys extruded at optimum speed and that of AZ31 alloy and Mg-0.2%Ce alloy [48].

3Al-0.4Mn) is a recently developed wrought magnesium alloy, which has a good balance of strength, ductility, extrudability [45]. As compared to AZ31 in Fig. 12(b), AM30 alloy offers up to a 50% improvement in ductility at temperatures up to $200 \text{ }^\circ\text{C}$, while maintaining similar yield and tensile strengths. Additionally, the maximum extrusion speed of AM30 is 20 to 50% higher than that of AZ31, resulting in improved extrudability as shown in Fig. 10(a).

Small additions of RE elements have been shown to be an effective approach for enhancing the mechanical properties of Mg alloys. Recent studies have reported a significant increase in elongation of pure magnesium with the addition of only 0.2% cerium [46]. The addition of Ce, similar to Y additions, has been found to enhance the slip of non-basal $\langle a \rangle$ dislocations [47]. However, the strength of Mg-0.2% Ce alloy is still low for structural applications. With further alloying with Zn, a new wrought Mg-2Zn-RE (ZE20) alloy with excellent extrudability was developed [48]. The addition of Zn provides solid solution strengthening, while the influences of both Zn and Ce are independently realized in these ternary alloys. Fig. 13a and b are electron backscatter diffraction (EBSD) inverse pole figure (IPF) maps showing that the grain size and morphology are nearly isotropic along both extruded direction and transverse direction in ZE20 tube walls extruded at $0.1 \text{ m}\cdot\text{s}^{-1}$. EBSD texture inverse pole figure in Fig. 13c indicates that the ZE20 microstructure has a component of the texture (termed R, or rare earth, texture component), corresponding to the c-axes of the grains oriented at an angle to the extrusion axis. Fig. 13d shows the comparison of mechanical properties among ZE20 alloy, AZ31 and other Mg-Zn-Ce based alloys. It can be seen that ZE20 alloy has an excellent balance of mechanical properties (135 MPa yield strength, 225 MPa ultimate tensile strength and 27% elongation) [48].

New Mg extrusion alloys have also been developed to achieve high yield strength. For instance, Pan et al. developed a new Mg-2Sn-2Ca (TX22) alloy with yield strength of 443 MPa [49]. However, it required a low extrusion temperature of $220 \text{ }^\circ\text{C}$ (thus, low speed) to achieve a fine microstructure. With increasing extrusion temperature, the yield strength is reduced as the grain size is increasing. To overcome this issue,

another new alloy Mg-5Al-3Ca-0.3Mn (AXM5303) presented a high YS of 420 MPa at a conventional extrusion temperature of $300 \text{ }^\circ\text{C}$ [50]. The addition of Ca leads to the formation of dense Mg_2Ca and Al_2Ca precipitates in both DRX and unDRX regions of AXM alloys, which promote the nucleation rate of DRX process, restrict the growth of DRX grains and promote the precipitate strengthening. Similar alloys, such as Mg-1Ca-1Al-0.3Zn-0.4Mn alloy (XAZM1100) and Mg-2.0Sn-1.95Ca-0.5Mn (TXM220) alloys are developed with the introduction of nano-sized precipitates during extrusion [51,52].

For high ductility/formability applications, Mg-Mn based alloys are showing attractive properties. The addition of Mn into Mg alloys can enhance the extrudability by increasing the solidus temperature of Mg alloys [53], providing a larger extruded temperature window. On the other hand, the low temperature extrusion leads to a fine DRXed microstructure due to the low migration rate of grain boundaries [54]. Moreover, the low extruded temperature results in a more obvious decrement of solubility of Mn in Mg matrix. It promotes the fine dynamic precipitation during extrusion and change the DRX mechanism from discontinuous dynamic recrystallization (DDRX) to continuous dynamic recrystallization (CDRX), which refines DRXed grain to less than $1 \text{ } \mu\text{m}$ with random texture [55,56]. The formation of fine microstructure leads to a high tensile ductility in Mg-Mn based alloys. For instance, Hidetoshi et al. reported a high room temperature ductility of 145% in extruded M-0.3 at%Mn alloy [57]. For the formability, the new developed Mg-0.5Mn-Al alloy is reported to achieve an exceptional rollability at room temperature. This alloy can be cold rolled at room temperature to a thickness of $\sim 1 \text{ mm}$ with an incredible large single pass reduction of 80% [58].

On the other hand, the ductile Mg-Mn alloys are usually with relatively low mechanical strength. To overcome this shortage, Mg-Mn alloys are alloyed with a third element, e.g., Al [59], Zn [60], Sn [61], Ca [60], Sc [62] and Gd [63] to promote their mechanical strength. Besides the addition of alloying elements, introducing inhomogeneous microstructure in extrusion or rolling process can also effectively further enhance their mechanical strength [55,63,64]. The inhomogeneous

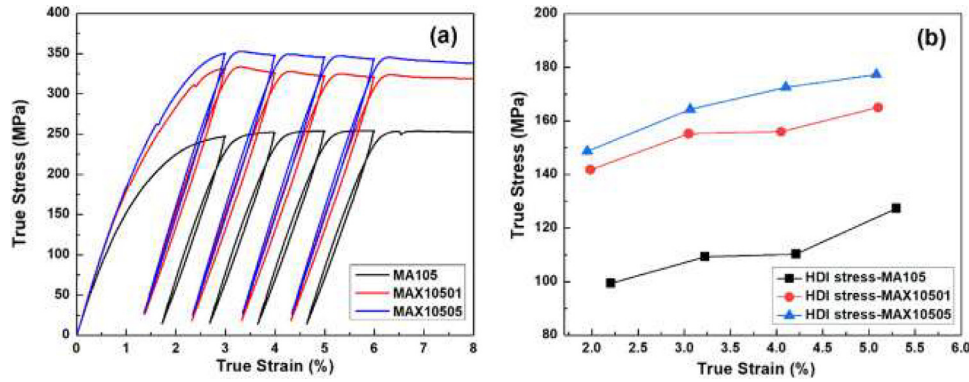


Fig. 14. (a) Loading-unloading-reloading (LUR) tensile curves of MA105, MAX10501 and MAX10505 samples and (b) the measured HDI stress determined from the LUR hysteresis loops [64].

geneous of grain size leads to an extra hetero-deformation-induced (HDI) strengthening, which provides a new strategy for mechanical performance in Mg alloys, seeing in Fig. 14.

3.3. Sheet Mg alloy development

Mg alloy sheets have great application potential to replace steel or Al alloys for automobile inner panels. However, unlike Al and steel sheet alloys, which can be easily fabricated into final shapes through stamping or other forming processes at room temperature, Mg alloy sheets exhibit poor formability at room temperature. Currently, sheet forming process of commercial Mg alloys generally needed to be conducted at elevated temperatures around 300 °C, which would greatly increase processing cost. Therefore, developing new Mg sheet alloys and novel processing routes to enhance the formability of magnesium alloy sheets at room temperature is critical for reducing processing costs and improving productivity. Besides micro-alloying with rare-earth alloying, the minor addition of non-rare earth (RE) elements, such as Ca, Zn, and Al also can improve the ductility and formability of Mg alloys. The addition of Ca to Mg alloys can increase the slip activity of non-basal $\langle a \rangle$ dislocation slip and thus improve ductility [65]. A recent study showed that the addition of Zn and Ca can increase the critical resolved shear stress (CRSS) for basal $\langle a \rangle$ slip and enhance the slip of non-basal and cross-slip of $\langle a \rangle$ dislocations between basal and prismatic planes [66]. Addition of Zn and Ca also weakens the basal texture and forms TD-split texture similar to those observed in Mg-Zn-Ce alloys [67,68].

Recently, lean Mg alloys with micro-additions of Ca, Zn or Ce, such as ZXEM2000 (Mg-2Zn-0.3Ca-0.2Ce-0.1Mn) [69], have been developed to offer room-temperature formability. However, these alloys generally have low post-forming strength due to limited strengthening phases in their microstructure. Among various strengthening mechanisms for Mg, precipitation strengthening can be most effective [70]. The development of heat-treatable Mg sheet alloys with superior formability at room temperature, coupled with rapid age-hardening characteristics, provide a promising strategy

towards extending the application of sheet Mg alloys. To achieve this objective, a novel Mg sheet alloy, ZAXME11100 (Mg-1.0Zn-1.0Al-0.5Ca-0.4Mn-0.2Ce), has been developed [71]. EBSD IPF map in Fig. 15a shows the microstructure of ZAXME11100 alloy after hot rolling followed by the solution treatment at 410 °C for 1 hour (designated as T4). The average grain size was measured to be about 9.6 μm based on EBSD results. Corresponding texture pole figures are given in Fig. 15b. The microstructure of ZAXME11100 has a weak TD-split texture. In the (0001) pole figure, the maximum texture intensity tilts about 40° away from the normal direction (ND) toward to the transverse direction (TD). Previous studies has shown that Zn and Ca addition can weaken basal texture and result in the formation of TD-split texture [55,56].

Fig. 16a show the aging hardening response of ZAXME11100 alloy at 210 °C. The alloy reaches peak aging hardness after aging at 210 °C for 1 hour (designated as T6 treatment). The ZAXME11100 alloy after T4 treatment exhibits a moderate yield strength (YS) of 159 MPa and an ultimate tensile strength (UTS) of 253 MPa with an extraordinarily high elongation of 31% and Index Erichsen (IE) value of 7.8 mm. After the T6 heat-treatment, the yield strength (Y.S.) and ultimate tensile strength (U.T.S.) have been significantly increases to 270 MPa, an approximate 70% increase in yield strength as compared with that of T4 condition, while its ductility only suffer a small reduction as shown in Fig. 16b. Fig. 16c and d summarize the engineering stress as a function of IE values as well as engineering strain for various Mg alloys and commercial Al sheet alloys. Fig. 17 plots IE value vs. yield strength at RT for AZ31 and various alloys evaluated by a United States Automotive Materials Partnership (USAMP) team [72]. Compared to commercial AZ31B alloy, ZEK100, E-Form Plus and ZXEM2000 all show improved room-temperature formability, but with slightly reduced yield strength. The new sheet alloy, ZAXME11100, offers both excellent ductility (31% tensile elongation) and RT formability (7.8 mm EI) in the solution-treated condition (T4), but with an extraordinary high yield strength (270 MPa) upon post-forming aging treatment (T6). The excellent combination of strength and formability of this new magnesium alloy, com-

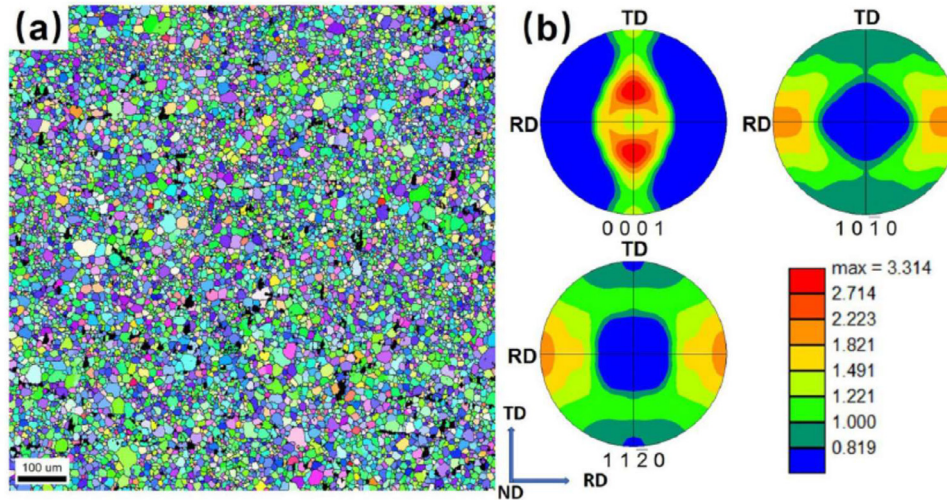


Fig. 15. (a) EBSD IPF map of ZAXME11100 alloy after forming solution treatment (T4) at 410 °C for 1 hour and then water quenching, (b) texture pole figures [71].

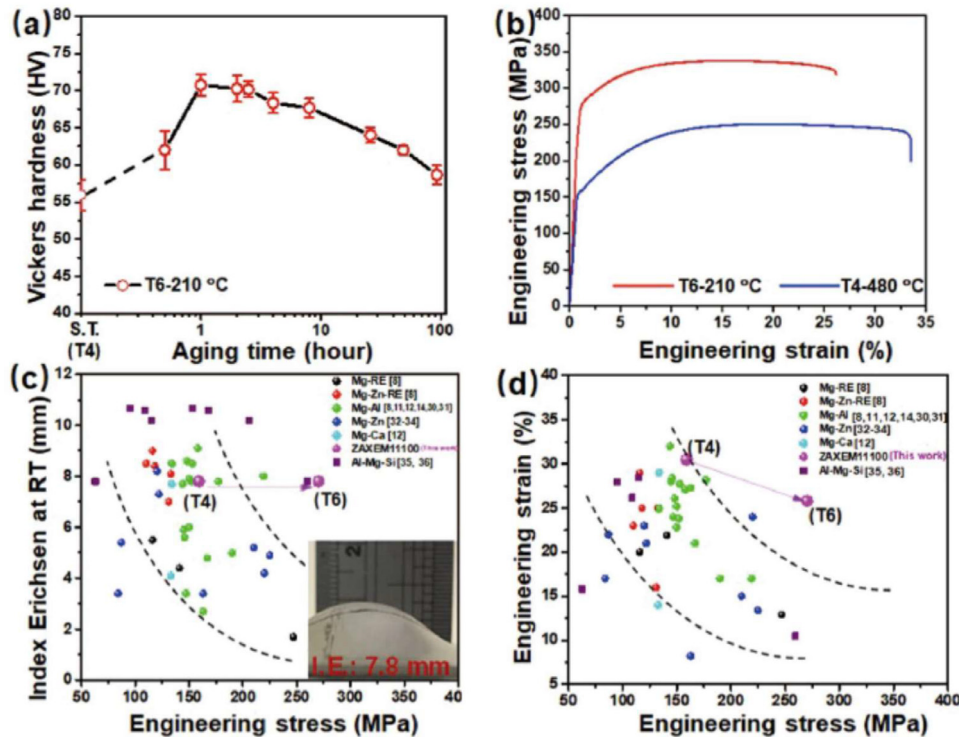


Fig. 16. (a) Age hardening response at 210 °C; (b) tensile curve from the T4 and peak-aged T6 treated ZAXME11100 alloy samples; (c) plot of I.E. at RT value as a function of engineering stress; (d) plot of engineering strain vs engineering stress at RT [71].

parable to those of 6000 sheet aluminum alloys (AA6016 and AA6061), clearly shows potential for room temperature forming of automotive applications [72].

4. Recent advances in magnesium process development

4.1. Solidification and grain refinement

Generating fine, equiaxed and non-dendritic grain structure during solidification is an important first step in achiev-

ing isotropic mechanical properties and minimizing the risk of casting defects such as shrinkage porosities, segregation and hot cracking. The addition of Zr to pure Mg and Al-free Mg alloys is regarded as the most effective way for grain refinement. The solubility of Zr in Mg and Mg-Y-Zr alloys, and its mechanical properties can be traced back to 1950's [73] and the grain refinement effect of Zr in Mg has been broadly reviewed [74]. The current practice is to add Mg-Zr master alloys where the undissolved Zr exists as particles and the solubility was estimated to be 0.44–0.50% (when added

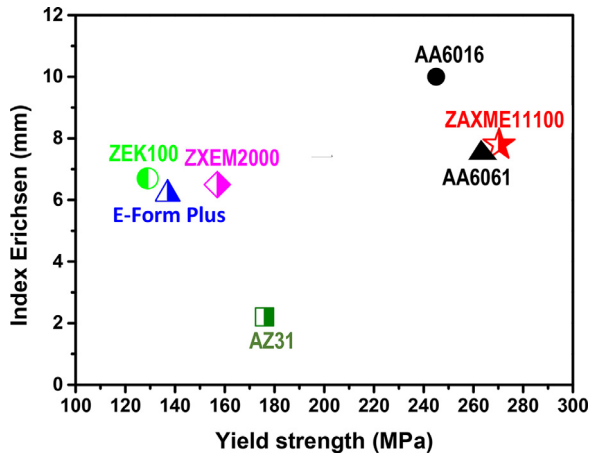


Fig. 17. RT formability (Index Erichsen value) vs. yield strength of various new Mg alloys in comparison with commercial Mg alloy AZ31B and Al alloys 6061 and 6016. For age-hardening ZAXME11100, AA6061 and AA6016 alloys, the EI was measured at T4 temper, while the yield strength is tested at T6 conditions [72].

greater than 0.5% in hyper-peritectic composition) [75,76]. Having an excellent crystallographic compatibility with Mg matrix, insoluble Zr acts as heterogeneous substrate for nucleation and solute Zr with highest growth restriction factor (Q) in Mg, leading to a remarkable grain size refinement in slow cooling conditions. However, this refining tendency of Zr is poisoned when trace amounts of impurities such as Fe, Mn, Si, Sn, Ni, Co, and Al are present, making this refiner ineffective for the most popular Mg-Al alloy system [77,78]. Secondly, the density difference between Mg and Zr at melting and casting temperatures causes a significant loss of Zr by sludge formation. To compensate the sludge, excess Zr addition is needed to produce the desired refinement in Zr containing Mg alloys [75,77]. Molten metal processing using intensive shearing [79] or ultrasonic treatments [75] have increased the number of active nucleation particles and reduces sludge formation. Tong et al. [80] treated the Mg-Zr master alloy using ultra-high frequency tungsten inert gas arc melting process and evaluated the grain refinement in Mg-9.0Gd-3.0Y alloy. Due to the very high cooling rate of the arc-melting process, the large size Zr agglomerate (1–20 μm) were reduced to nano-size precipitates (below 1 μm) and showed excellent grain refinement by a further improvement of 41–47% than the conventional master alloy.

For Mg-Al based alloys, there is no satisfactory approach for grain refinement [81], except for carbon inoculation, adding titanium [82] or SiC particles [83] which can provide some grain refinement effects. A recent work by Zhang et al. [84] investigated the grain refinement of AZ31 alloy by a Mg-Ca-Sn master alloy that contains mainly Mg and CaMgSn phase (by fixing the mass ratio of Sn to Ca as 3). The average grain size of 270 μm was significantly reduced to less 90–100 μm and identified that the CaMgZn particles act as potential heterogeneous nucleation sites, shown in Fig. 18.

For future research in Mg grain refinement, the following thoughts are put forward. Although alloy chemistry modifi-

cation has been widely used to promote refinement of microstructure during solidification, there are several limitations associated with this approach:

- 1) Alloying elements/impurities: Interaction of a grain refiner with either an alloying element or trace amounts of impurities could lead to a dramatic loss of refinement tendency by forming other stable intermetallics at high temperatures. For this reason, Zr refinement works with Mg-RE alloys and becomes an inefficient refiner for Mg-Al based alloys [77,81]. Impurities generally present in trace amounts such as Fe or Mn have been reported to sometimes assist and other times poison/reduce the efficiency of C-based grain refiners [81].
- 2) Addition methods/distribution of particles: Grain refiners are generally added in the form of master alloys. Earlier methods have reported the use of gas bubbling methods [77], however, one of the key issues is the effective distribution of grain refiners. Addition of SiC to Mg-Al and Mg-Zn alloys have been found to work satisfactorily [85], while the consistency is severely affected by the added amount, particle size, addition methods and impurities in the alloy. The addition of SiC is generally very small to avoid making a metal matrix composite which would affect the properties of the base alloy.
- 3) Active particles: It has been estimated that in conventional conditions and for a given distribution of particles added through master alloy, only 1% of the added particles are active in grain refinement. This can be further increased by cooling conditions and external melt shear or ultrasonic processing to 3–4% [86]. Recent research has been focused on understanding the role of nucleation stifling mechanisms such as solute suppression zone (SSN) or nucleation free zone (NFZ) or inhibited nucleation zone (INZ) [77,86,87]. Solute and thermal gradients during solidification play significant role in both activating and stifling a nucleation particle.

Prominent reviews by StJohn and Easton [77] and Karakulak [81] summarized the grain refinement mechanisms and newly developed refiners for Mg-Al alloys. Identifying potent refiner for Mg-Al alloys, specifically gravity cast AZ91 alloy has been one of the most intensively researched and is still an active area for research. Oxide particles [88], carbide [85] and boride-based [89] particles are some of the notable current topics in this research. To overcome the limitations associated with alloy chemistry modification, physical methods have been investigated to refine the grain size during solidification. Notable processing methods include melt stirring or intensive shearing, electro-magnetic and ultrasonic treatments [90]. Following are the additional benefits of external field processing of molten/solidifying metals.

- 1) Improved wettability of suspended heterogeneous particles and native un-wetted oxide particles thereby increasing the total number of active sites for grain refinement [79].

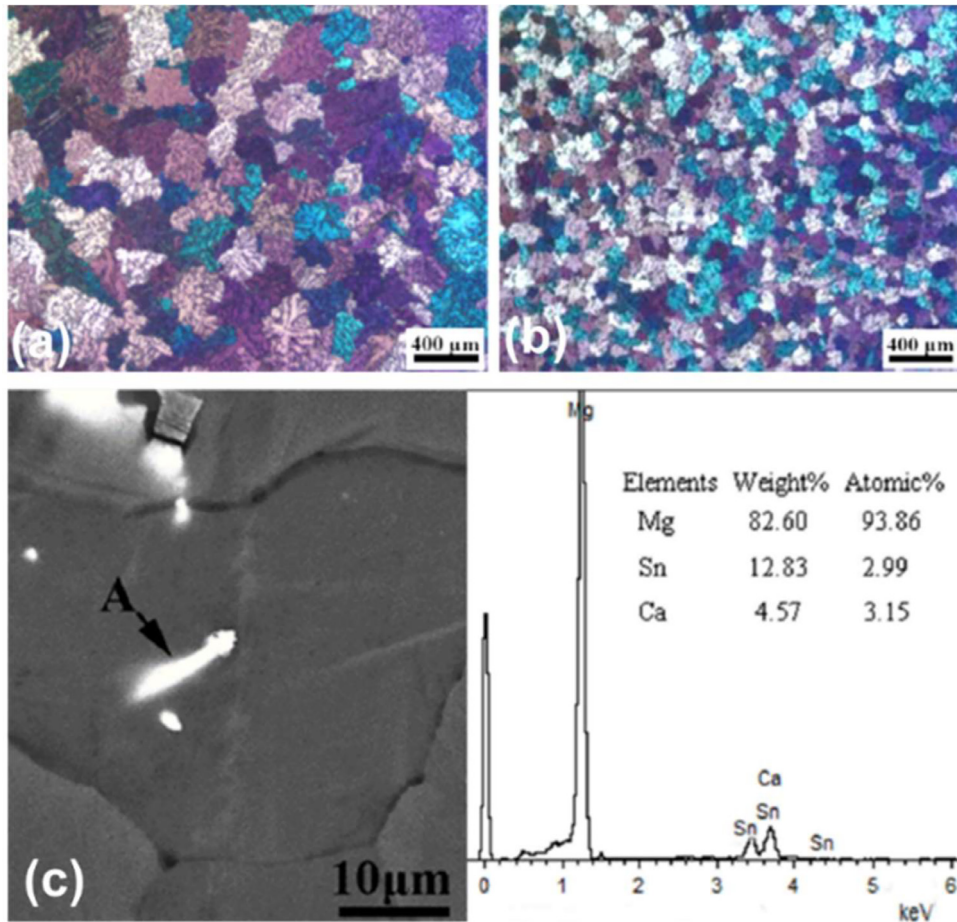


Fig. 18. Grain refinement of AZ31 (a) without refiner and (b) after the addition of 0.75 wt.% CaMgSn alloy. (c) SEM and EDS analysis of bright CaMgSn particles located in the center of the grains identified as potential nucleation sites [84].

- 2) Intense forced convection generated external forces induces melt flow and reduces steep temperature gradients during solidification, enabling more nucleation and reduces the macro-segregation of second phases in large ingots [90].
- 3) Physical forces either mechanical or fluid flow can cause fragmentation of dendrites, removal of free crystals from the melt surface and mold walls [90]. Additionally, cavitations induced by ultrasonic processing can produce fragmentation, bending and breaking of dendrites together increasing the number density of grains for equiaxed grain structure [91].
- 4) Besides grain refinement, ultrasonic processing has been demonstrated for degassing of melts and refinement of primary intermetallic phases for enhanced mechanical properties of both Mg and Al alloys [92,93].

Dedicated reviews for external field processing explains the fundamental mechanisms on the origin of fine grains during ultrasonic, magnetic and stirring methods applicable to Al and Mg alloys [90]. Melt processing techniques such as intensive stirring and semi-solid processing can enhance grain refinement. The developments in chemical and physical approaches

for grain refinement shed more insights on the mechanism of grain formation, more efforts are needed identify a potential refiner for consistent performance and maximize the efficacy of current grain refiners to widen the applications of cast Mg alloys.

4.2. Vacuum die casting

As discussed in an earlier review published in this journal [94], die casting, generally referred as high pressure die casting (HPDC), is the dominant manufacturing process for Mg applications due to its low cost and high productivity. Depending on the applied pressure and other control mechanisms, this process can be classified as cold-chamber HPDC, hot chamber HPDC, vacuum die casting and semi-solid Rheo- or Thixo-casting process. The use of vacuum during die casting to assist die filling has been quantitatively proven to improve thin-wall capability and reduce porosity (air entrapment) in HPDC castings [95]. Vacuum die casting is thus extensively used to produce thin-wall die castings for automotive body structures, especially in electric vehicles. With the increasing use of large Al castings (mega-casting) in the automotive industry, it is expected that similar Mg castings will be devel-

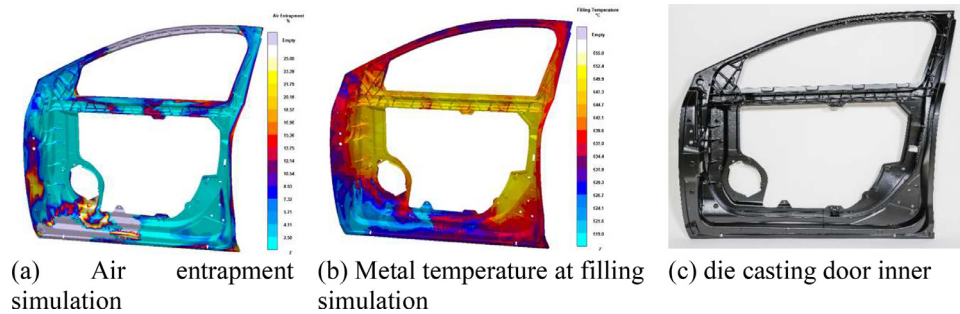


Fig. 19. (a) and (b) Advanced casting process simulations; and (c) die cast door inner.

oped using advanced vacuum die casting. A recent example of thin-wall Mg die casting was a 2.0 mm-wall door inner with significant mass reduction (46%) and part consolidation compared to steel door design. Fig. 19 shows advanced casting simulations and a Mg door inner casting [96].

4.3. Squeeze casting

The generic term squeeze casting (SC) refers to the combination of metal-casting process along with forming operation (also called as liquid metal forging) to fabricate near-net shaped products. The liquid metal is poured over the bottom half of the mold, usually reusable, preheated die which is then closed by the top half of the mold enabling the pressure-tight mold filling. Solidification proceeds under pressure (~50–140 MPa) facilitating high-yield castings with fewer defects when compared to gravity or HPDC components [97]. Depending on the nature of applying pressure to the solidifying metal, this can be further classified into direct or indirect squeeze casting process and the intensification stage can be applied either at the onset or after the crystallization [98]. Several improvements are noted in terms of mechanical properties, reduced porosities, refinement of second phases and grains and fabrication of metal matrix composites applicable to Mg alloys [99–101]. The role of applied pressure (ΔP) on the microstructure enhancement is explained by Clausius-Clapeyron criterion:

$$\frac{\Delta T}{\Delta P} = \frac{\Delta V \cdot T_m}{\Delta H_f} \quad (3)$$

where ΔV is the change in specific volume, T_m is the melting temperature of the alloy and ΔH_f is the latent heat of fusion. A comparison study of SC AZ91 showed minimal porosity, refinement of $Mg_{17}Al_{12}$ phase and better tensile properties to that of the gravity cast alloy [36]. Addition of Ca increased the creep strength of the SC AZX911 alloy due to the formation of thermally stable Al_2Ca phase network restricting the movement of dislocations [100]. Significant improvements are also noted in RE containing SC Mg alloys such as GW103K at temperatures up to 300 °C where the reduction in micro porosity in the as-solidified structure and micro-void coalescence delayed the propagation of cracks than the gravity cast alloy [101]. In addition to the conventional SC process, rheo-assisted SC have been reported in AZ91 alloy with Ce and

Ca for the refinement of microstructure and better mechanical properties of alloys [102]. A biodegradable Mg-4Zn-0.5Ca-(0–0.8)Mn alloy (compositions in wt.%) has been reported by Cho et al. [42,103] uses CALPHAD approach to identify the phases formed in the alloys and the SC process showed refinement of grains and second phases. The yield strength, ultimate strength and elongation increases linearly from 202 to 280 MPa, 115 to 201 MPa and 15% to 22% respectively when Mn is increased to 0.8 wt.%. Uniform microstructure and the formation of stable protection layer improved the corrosion resistance. In vivo studies indicated a good biocompatibility without inflammatory response and showed increase cell viability [42].

4.4. Forming processes and processing maps

Advanced wrought processing techniques can help refine grain sizes and modify texture [104,44,105]. Weakened and modified basal texture can tailor the deformation anisotropy and yield asymmetry, thus contributing to ductility and formability [106–108]. In the past decades, many advanced processing techniques such as, high pressure torsion (HPT), equal channel angular processing (ECAP), constrained groove pressing and surface nanocrystallization have been developed to refine and modify the microstructure of magnesium alloys [109–112]. Those techniques mainly utilize severe plastic deformation. The major limitations for those techniques are complex experimental setup and costly for industrial scale production. Conventional thermo-mechanical processing such as extrusion and rolling are still most economical and efficient ways for large-scale production of wrought magnesium alloys. The properties of wrought magnesium alloys can be enhanced through optimization of thermo-mechanical processing parameters.

Processing maps based on dynamic materials models, consisting of power dissipation efficiency maps together with instability maps, are powerful tools for identifying optimal thermo-mechanical processing conditions and for microstructure control [113]. They can be constructed using hot compression test. When combining with detailed microstructure characterization, optimal processing conditions and microstructure with weak basal texture and fine grain size generated by dynamic recrystallization can be identified. Fig. 20a shows the processing maps of ZE20 alloy at 15% compression

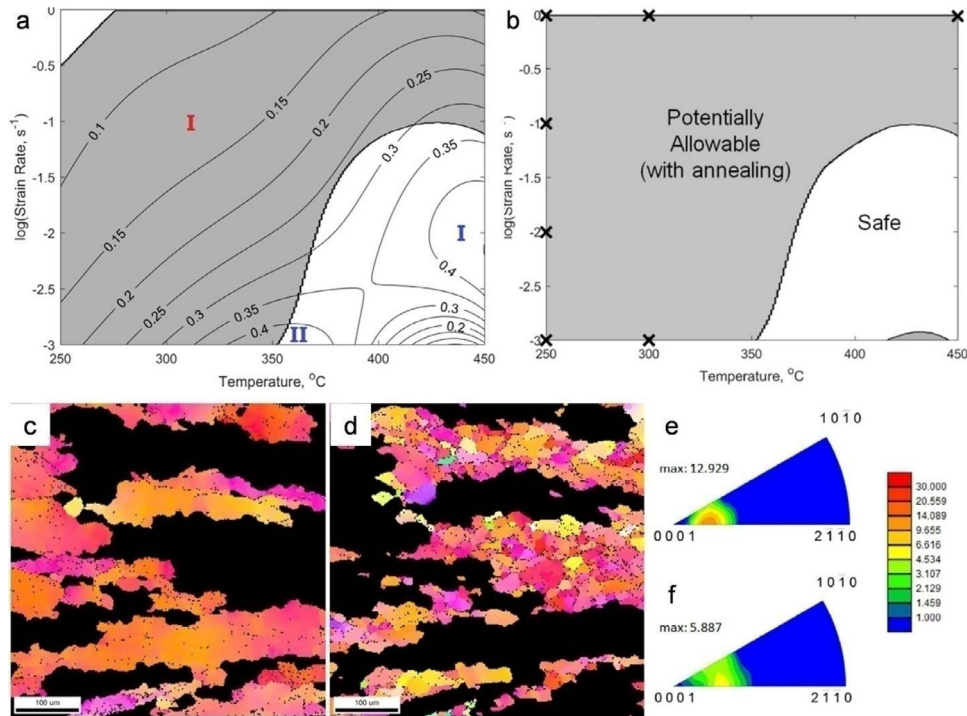


Fig. 20. (a) Processing map for ZE20 at 15% strain, (b) summary of processing conditions for ZE20. (Shaded areas indicate the presence of an instability region. X indicates conditions under which cracking was observed), (c) EBSD IPF in the compression direction of deformed grains of a specimen tested at 450 °C and 10^{-2} s^{-1} (Domain I) to 100% strain, (d) EBSD IPF in the compression direction of recrystallized grains of a specimen tested at 450 °C and 10^{-2} s^{-1} (Domain I) to 100% strain, (e) corresponding texture IPF of the deformed grains for the compression direction, and (f) corresponding texture IPF of the recrystallized grains in the compression direction [114].

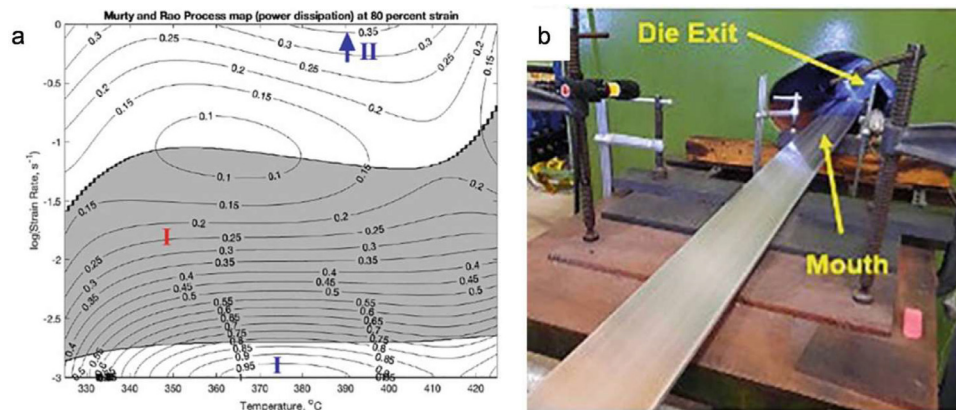


Fig. 21. (a) Processing map constructed for ZAXEM11100 at a 80% strain with the instability region shaded in gray. Contour lines correspond to lines of equal efficiency; and (b) Images of extruded ZAXEM11100 plate as it left the die with an extrusion speed of a 1"/min (25.4 mm/min) [115].

strain [114]. Optimized processing conditions for the alloy are highlighted in Fig. 20(b). High activity of dynamic recrystallization (DRX) was found between 375 °C and 450 °C, from 10^{-1} s^{-1} to $10^{-2.5} \text{ s}^{-1}$. Figs. 20(c) and (d) shows the EBSD characterization of the microstructure after compression. It can be seen high density of recrystallized grains were achieved. From the IPF maps in Figs. 20(e) and (f), it is seen that dynamic recrystallization can both refine grain size and also weaken basal texture, which will greatly benefit the ductility and formability. Fig. 21a shows the processing map constructed for ZAXEM11100 alloy at 80% strain. Based on processing map, a pilot extrusion test of the alloy un-

der industrial scale was successfully performed as shown in Fig. 21b [115].

5. Additive manufacturing processes

Additive manufacturing (AM), also known as 3D printing, is a cutting-edge technology that progressively adds thin layers of material based on 3D model data. This method is advantageous for fabricating complex geometries at fine resolutions and with complex geometry, which has gained significant attention in developing biodegradable implants [116,117]. Additive manufacturing of Mg alloys is of growing interest

due to its unique design capabilities, which are not achievable with traditional manufacturing methods [81,118,119]. Additionally, individualized implants that closely align with anatomical geometries can be produced while reducing manufacturing time, and cost as multiple steps of conventional machining may be eliminated [120–122].

Since the first reported study on AM of Mg in 2010 by Ng et al. [123], numerous AM experiments have been carried out on Mg alloys and composites [120]. However, the printability of Mg alloys is still the biggest challenge to achieving a sound AM part. Firstly, Mg has a high oxidation rate due to its high chemical reactivity, which makes it difficult to process and affects the dimensional accuracy and topology resolution of the printed parts [124]. Additionally, the high surface energy of Mg powders makes them more susceptible to react with atmospheric oxygen, causing combustion. Furthermore, the relatively low melting temperature (~ 650 °C) and the low boiling temperature (~ 1090 °C) of Mg impose severe evaporation during AM process, particularly for powder bed fusion (PBF) processes [120]. Moreover, the rapid growth of grain size directly affects the mechanical properties of the as-built component [125]. Despite these challenges, Mg AM has gained significant attention in recent years, and specialized equipment has been developed to create an inert atmosphere, ensuring safety in material handling [126,127]. So far, several AM techniques have successfully applied to Mg alloys, including laser powder bed fusion (LPBF), wire arc AM (WAAM), paste extrusion deposition, friction stir AM, and binder jetting process (BJP) [120,124,128]. Each method has its process mechanics and forms of raw materials, resulting in AM components with different microstructure and properties. Highly complex geometries that are difficult or impossible to manufacture using conventional machining processes can be developed by utilizing these techniques.

5.1. Mg powder production

To manufacture Mg products using powder-based AM techniques, the first and foremost challenge is to produce

high-quality (shape, size distribution, and chemical composition) Mg alloy powders. Unfortunately, the production of Mg powder is highly hazardous due to its reactivity and large surface areas. Currently, only pure Mg, AZ91 and WE43 powder are produced by a few manufacturers. Especially the powder manufacturing of bioabsorbable Mg-Zn-Ca-Mn alloy systems has not yet been widely explored or reported. Fig. 22 shows the preparation of Mg-Zn-Ca-Mn alloy powders for AM process using a compact induction gas atomizer. It is preliminary found that increasing the nozzle diameter significantly increases the size and distribution of the powder. Gas atomization was found to be highly effective in producing spherical powder, but the low viscosity and surface tension of Mg melt could lead to the powder becoming very fine during atomization. However, such very fine powders may attach or aggregate on some larger powder particles. Consequently, ongoing research is focused on increasing the yield of approximately 50 μm -sized Mg powder suitable for AM technology while reducing size distribution.

5.2. Laser powder bed fusion (LPBF)

LPBF utilizes a high-intensity laser beam that can be focused into small spots, with good precision in building 3D components. Laser beams are absorbed efficiently without any transfer medium, melting the powder followed by rapid solidification [129,130]. However, Mg alloys have low evaporation temperatures, with an evaporation point of 1090 °C for pure Mg, leading to possible composition changes in the material due to Mg evaporation during LPBF. Thus, the processing windows for LPBF of Mg alloys are generally limited [120,129,131]. Porosity is a common issue for most metallic materials, with several mechanisms related to gas pore formation [132] and alloy powders.

Overall, LPBF is a promising method for additive manufacturing of Mg alloys, with several challenges related to porosity, Mg evaporation, and cracking. The optimum processing window for each alloy system is crucial to achieving good quality parts. Further research is needed to understand

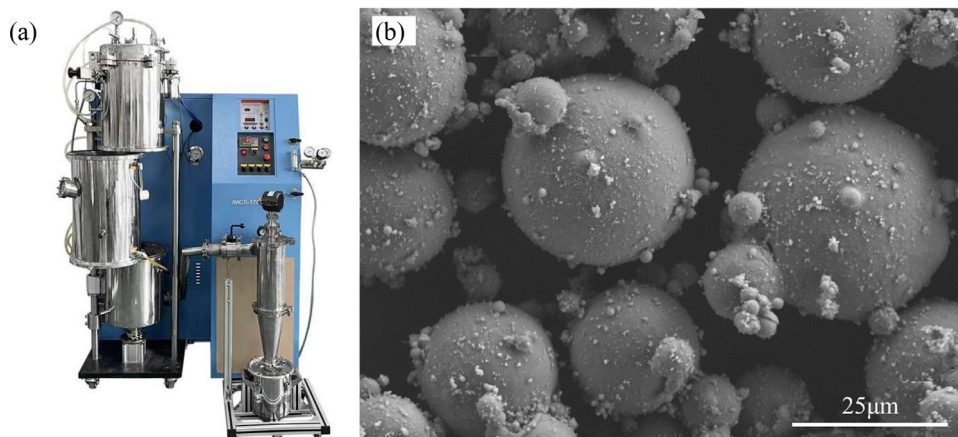


Fig. 22. The powder preparation and setup for Mg alloys at the Ohio State University: (a) Compact induction gas atomizer and (b) gas atomized Mg-Zn-Ca-Mn alloy powder.

the effects of alloying and processing conditions on cracking and porosity in Mg alloys during LPBF. Another important challenge is the residual stresses, which can be reduced by preheating of feedstock as well as post-printing heat treatment. Anisotropy of properties of built parts are also important issues which need more research and understanding.

5.3. Wire arc additive manufacturing (WAAM)

WAAM is considered an alternative method to laser or sinter-based additive manufacturing for Mg alloys. Unlike LPBF, WAAM uses Mg alloy wires as the feedstock material, allowing for high deposition rates, low equipment costs, and high material utilization, making it environmentally friendly [122]. Meanwhile, the use of Mg alloy wires in WAAM eliminates safety risks associated with Mg powder handling, and significantly reduces the costs of feedstock material production, transport, storage, and safety management.

However, major drawbacks of WAAM include coarse grain size, limited availability of wires (e.g., no custom alloys), gas contamination, thermal deformation, and the sophistication of the processing. Currently, cold-metal-transfer (CMT) is the most suitable WAAM technique for Mg alloys since CMT welding generates only one-tenth of the heat of MIG welding [130,133]. To date, wire-based processes for Mg alloys have not been widely used due to insufficient wire availability. WAAM processing of AZ31 [134–136], AZ61 [137], AZ80 [138,139], AZ91 [133,140], and AEX11 [141] has been reported. Other drawbacks of WAAM compared to other AM methods, include rougher built surfaces and lower dimensional accuracy. Post-WAAM machining and surface finishing are necessary, limiting its applications in many industries. Scaffold structures from WAAM might be too coarse for applications in medical. Overall, WAAM is a promising method for AM of Mg alloys, with several challenges related to surface roughness, dimensional accuracy, and availability of custom alloy wires.

5.4. Binder jetting process (BJP)

Binder jetting is a two-step AM process which includes 1) printing the green parts with needed shape; and 2) transforming into a densified parts [142,143]. In the first step, the alloy powders are bonded into the required shape and structure by binder, since this step is operated at room temperature, so the alloy powders will not have severe oxidation even in the air atmosphere. In the second step, printed green parts are sintered under the protective atmosphere and without severe oxidation reaction too. This step involves the debinding process and the densification process by sintering, hot isostatic pressing. Therefore, compared with other AM processes, two-step AM is particularly suitable for additive manufacturing the active alloys such as Mg alloys.

The biggest challenge in binder jetting AM of Mg alloy is the difficulty to densify the printed parts because Mg powders can easily form MgO film on the surface [143–145]. Unlike Fe and Cu, the Mg diffusivity in its oxide is sev-

eral orders of magnitude lower than its self-diffusivity, so the MgO film will resist exceedingly to mass transport and forming a sintering neck between Mg alloy powders in solid-state sintering process. Recently, Su et al. [145,146] evaluated the mechanical and corrosion properties of Mg alloys manufactured using a full-liquid sintering method, which significantly reduced the sintering time to produce high-quality final products via a binder jetting process. This method allowed for the creation of dense and fully consolidated parts with complex geometries through the selective melting and solidification of the alloy powder. The results of these studies demonstrated that the sintered Mg alloy exhibited good mechanical properties, with comparable or even superior strength characteristics compared to conventionally manufactured Mg alloys.

Additionally, BJP is a promising route for fabricating highly interconnected porous Mg structures with a wide range of pore sizes and pore morphology [144]. However, the introduction of porous structure also leads to higher corrosion rates due to the increased surface area [143] and crevice corrosion [147]. More research is needed to better understand the relationship between the printing parameters on porosity and their corresponding corrosion performance.

5.5. Friction stir-based AM

Friction stir-based AM is a solid-state technique that uses friction stir welding to additively manufacture large-scale near-net-shaped components [148,149]. Basically, it is a solid-state processing method that involves using a rotating tool to generate frictional heat, plasticize the material, and induce mixing and consolidation without complete melting. There are two methods of friction stir-based AM: friction stir additive manufacturing (FSAM) and additive friction stir deposition (AFSD). In FSAM, multiple-plate stacks are welded together using a non-consumable rotating tool; while in AFSD, feed materials are pushed to the stir zone through a non-consumable hollow cylindrical tool [150]. The benefits of friction stir-based AM for Mg alloys include the ability to render relatively dense builds with fine and equiaxed microstructures and enhanced mechanical properties, such as higher tensile strength, improved fatigue resistance, and increased ductility due to reduced porosity and modified grain size [150,151]. Operating processing windows are controlled by key parameters such as tool rotational speed, traverse speed, plunge depth, geometries, and feed rate to obtain sound structures. However, major drawbacks of FS-based AM are its inability to fabricate complex geometries, spatial resolution, and geometric precision. Therefore, the design freedom for friction stir-based AM is relatively limited, which requires further development of FS-based AM equipment and process innovations.

6. Integrated computational materials engineering (ICME)

Integrated Computational Materials Engineering (ICME) is defined as “the integration of materials information, cap-

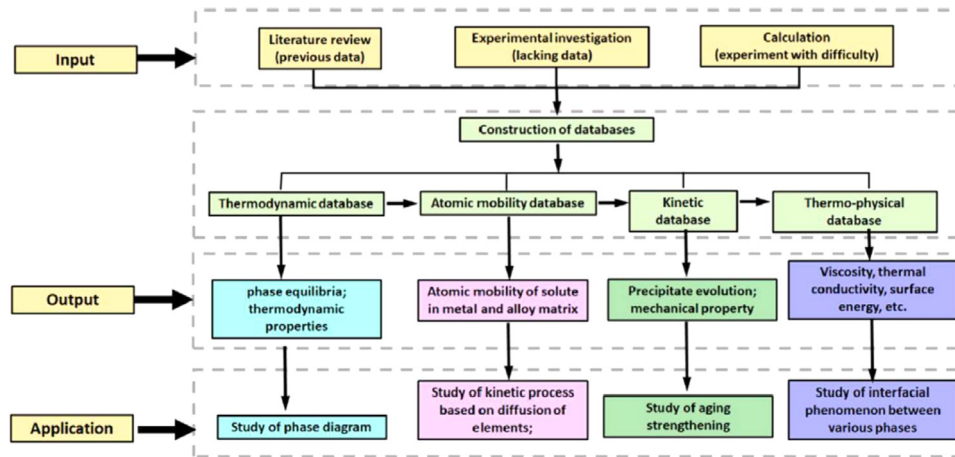


Fig. 23. Schematic overview of extended CALPHAD methodology in the framework of ICME [156].

tured in computational tools, with engineering product performance analysis and manufacturing-process simulation,” according to a United States National Research Council study [145]. Within an ICME framework, materials models and process models of multi-length scales can be integrated to accelerate the design and manufacturing of engineering products [152–154]. Compared to other engineering alloys such as steels and Al alloys, the industrial applications of Mg alloys are limited by both the scarcity of high-performance alloys and the high processing costs involved. To overcome these obstacles, ICME offers great potential to accelerate the development of novel Mg alloys and optimize their processing.

6.1. ICME for Mg casting

Currently, over 90% commercial Mg alloy components are produced using die casting, especially high pressure die casting [34]. Therefore, the development of ICME of Mg castings is crucial for their industrial applications. The CALculation of PHase Diagrams (CALPHAD) method was originally developed for the construction of phase diagrams based on phase equilibrium calculations and thermodynamic properties of complex multi-component, multi-phase systems. It has been extended to cover a wider range of applications, such as simulating solidification and precipitation phenomena [155]. The combination of CALPHAD simulation with other physical property databases and models has led to its extensive use in property modeling as illustrated in Fig. 23 [156]. Consequently, CALPHAD simulations have become the core modules of ICME of Mg alloys for casting applications.

6.2. Development of thermodynamic databases

Accurate and comprehensive thermodynamic and kinetics databases are essential to CALPHAD based modeling. The traditional approach to develop the thermodynamic databases relies on critical experimental data, which usually involve tedious experimental work including alloy preparation, homogenization heat treatment, and characterization of crystal struc-

tures and phase compositions of constituent phases. The main drawback of traditional approach is often costly and inefficient in collecting experimental thermodynamic data, especially thermo-chemical data. The incompleteness of experimental data often results in uncertainties in thermodynamic modeling. Fortunately, contemporary computational tools, such as those based on first-principles calculations utilizing density functional theory, substantially contributed to the development of thermodynamic databases [157,158], making them a vital aspect of computational thermodynamics. Fig. 24(a) and (b) show the examples of calculated isothermal section of Ca–Mg–Sr ternary system [159] and Mg–Ca–Ce system [160], which were evaluated by the combination of computational thermodynamics with first-principles calculations modeling. Moreover, recently, to fill out the gaps between experimental data and modeled data, a user-friendly, extensible, self-optimizing phase equilibrium infrastructure (ESPEI) for Mg alloys were developed. ESPEI integrates databases (crystallographic, phase equilibrium, thermo-chemical, and modeled Gibbs energy data) and database development (automation of thermodynamic modeling) with GUI, making the material research and development more efficient [161]. With both experimental and computational efforts, Mg thermodynamic databases in commercial CALPHAD packages including PanMg (Computhermo) and TCMg (Thermo-calc) have been greatly extended to include over 30 alloying elements, which provide a powerful tool for ICME-base Mg alloy simulation.

6.3. Development of kinetic databases

Kinetic databases, consisting of diffusion coefficients and mobility, are crucial for reliable simulations of ICME process modeling such as solidification, heat treatment, and precipitation. However, compared to the thermodynamic databases, the kinetic databases for Mg alloys are less developed. Traditionally, diffusion multiples have been the primary experimental method for collecting diffusion data, but their applicability is limited to certain elements, such as Al and Ca, which lack

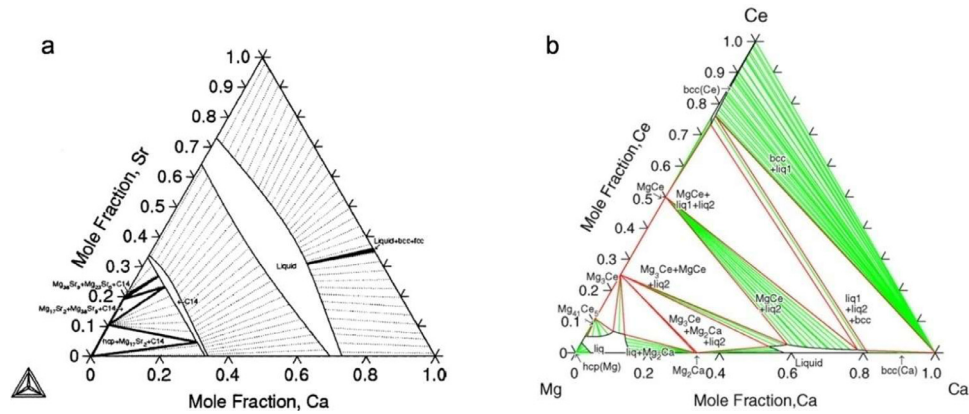


Fig. 24. Thermodynamic assessments Mg alloys using CALPHAD approach complemented by first-principles calculations: (a) calculated isothermal section of Ca-Mg-Sr system at 750 K. The dotted lines are the tie-lines [159], (b) calculated isothermal section for the Mg-Ca-Ce system at 880 K [160].

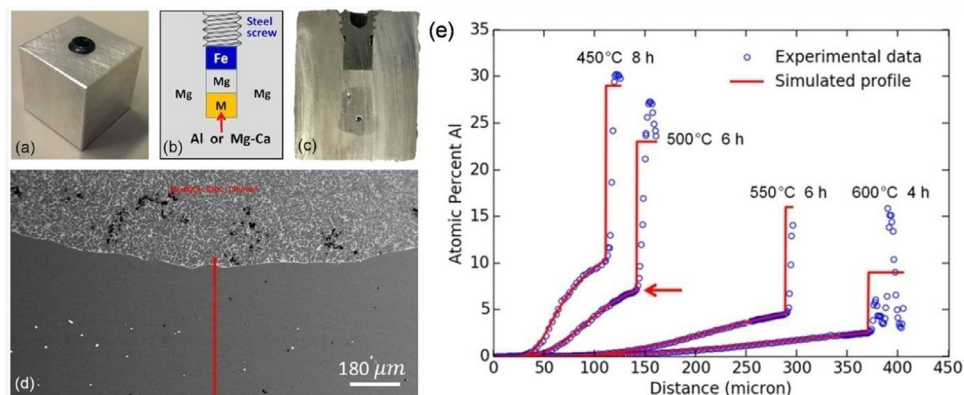


Fig. 25. (a) Photo of a LSDC ($\sim 20 \times 20 \times 25$ mm), (b) schematic illustration of the cross section of a LSDC, (c) an example of a LSDC after diffusion heat treatment showing its melted/liquid region after the sample was quenched to room temperature and sectioned, (d) SEM image of the liquid-solid boundary of a Mg-Ca LSDC that was diffusion annealed at 630 °C for 13 h and then water quenched to room temperature. The solidified liquid phase pool is on the top and the solid-solution is at the bottom, (e) comparison of experimental and simulated concentration profiles at four temperatures in Mg-Al LSDCs [162].

suitable radioactive isotopes. Furthermore, exact alloy compositions of extremely dilute Mg alloys containing elements such as Ca, Sr, and Nd pose a challenge to diffusion multiple experiments.

Recently, a novel liquid-solid diffusion couple (LSDC) geometry has been developed which takes advantage of the liquid phase formation at annealing temperatures above the eutectic point [162]. This method involves creating a small liquid pool inside a relatively large block of pure Mg. Fig. 25(a) shows an example of LSDC. EPMA (Electron Probe Micro-Analysis) was widely employed to measure concentration profiles across the interface. The forward simulation method can be utilized to extract impurity diffusion coefficients from experimental composition measurements. Fig. 25(b) displays a comparison between the experimental composition profiles measured using EPMA, and the corresponding results obtained from forward simulations. Given the aforementioned challenges associated with experimental measurements of diffusion coefficients in Mg, first-principles calculations have been extensively conducted in recent years to evaluate the mobilities of alloying elements in Mg [163]. To establish the most comprehensive mobility database to date, a systematic

analysis of all experimental and computed diffusion data in Mg has been conducted to assess the mobility of 22 alloying elements in Mg [164]. Fig. 26 shows an example of assessed mobility of alloying elements. Such mobility databases will be a valuable contribution towards the development of the kinetic databases for ICME of Mg alloys, and will aid in the future development of high performance Mg alloys using ICME approaches.

6.4. Modeling solidification microstructure

Among different casting methods, high pressure die casting (HPDC) is especially favored for producing thin-walled and complex Mg components in an efficient and economical manner. The cooling rates associated with HPDC are extremely high, typically ranging from 100 to 1000 °C/s, leading to solidification conditions in Mg products that are far from equilibrium. As a result, microsegregation and the redistribution of alloying elements can occur, which significantly affect local microstructure and the homogeneity of mechanical properties. To address this issue, a simulation tool for predicting solidification microstructure and microsegregation be-

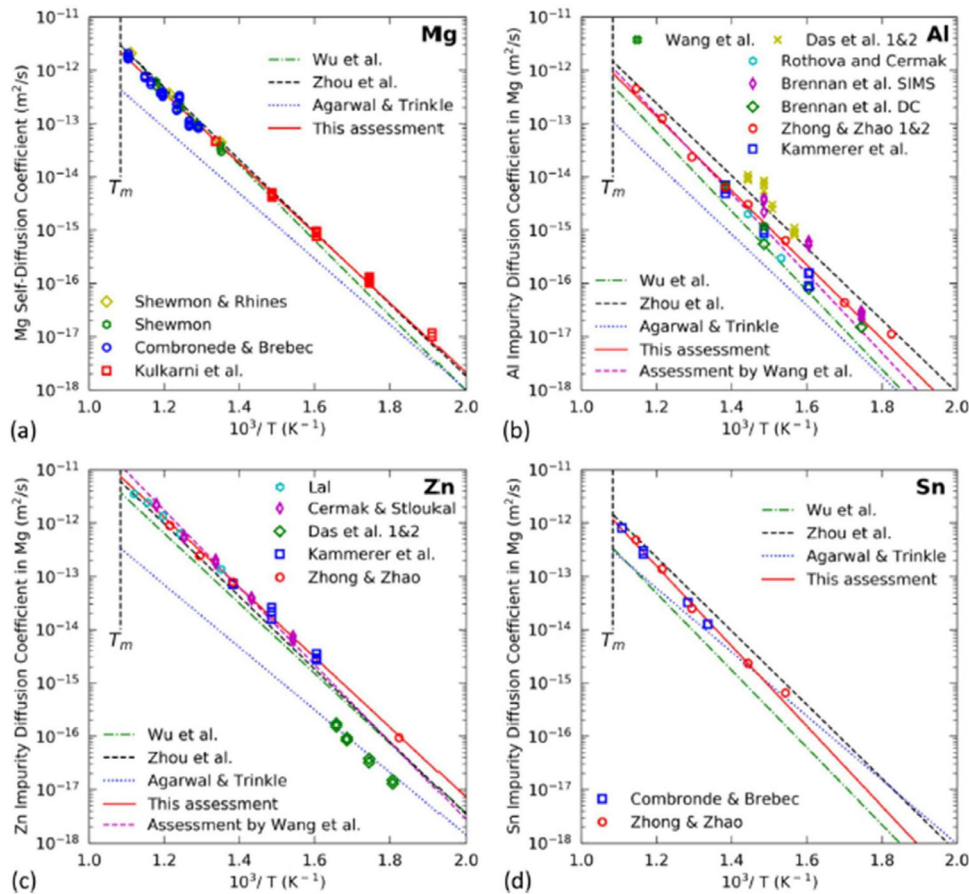


Fig. 26. Assessment of mobility of dilute diffusion coefficients in Mg in comparison with all available experimental data and first-principles calculation: (a) Mg, (b) Al, (c) Zn and (d) Sn [164].

comes a crucial component of ICME of Mg alloys. The conventional non-equilibrium Scheil-Gulliver model is inadequate for predicting the solidification microstructure evolution and the redistribution of alloying elements during HPDC of Mg alloys, which normally involves back diffusion. In a recent study, a CALPHAD-based solidification micro-model was developed to predict the solidification microstructure of multi-component Mg alloys, including secondary dendrite arm spacing (SDAS), microsegregation, and non-equilibrium phases [165]. The model incorporates back diffusion in the solidified primary phase, as well as undercooling and dendrite arm coarsening during solidification. Fig. 27 shows an example of such model in simulating secondary dendrite arm spacing (SDAS) and microsegregation of Al and Sn in Mg-7Al-2Sn alloy. Good agreement were achieved between experimental measurements and simulated results. This study highlights the potential of using the CALPHAD-based solidification micro-models as a valuable tool in the ICME of Mg alloys, particularly in predicting and optimizing the microstructure and properties of Mg casting components.

6.5. Modeling precipitation microstructure

One of the most effective techniques for enhancing the strength of Mg alloys is precipitation strengthening, which de-

pends on the characteristics of the precipitates, such as their types, sizes, number density, and volume fraction. Precipitation modeling techniques such as phase field method are valuable for studying the evolution of the size, morphology and variant selection of precipitates in Mg alloys in small modeling domains [166,167]. Such techniques are difficult to be coupled with CALPHAD databases for simulation of the evolution of large volume fraction of precipitates for industrial applications. Numerical method such as Kampmann-Wagner numerical (KWN) model has garnered significant attention due to its ability to effectively simulate concurrent nucleation, growth, and coarsening kinetics of precipitates [168,169]. The KWN model can be coupled with thermodynamic and kinetic databases, as well as other microstructural models, to predict the evolution of precipitation in multi-component and multi-precipitate Mg alloys [170,171]. In the original KWN model, precipitates were assumed to be spherical, which differs from the real situation in which most precipitates in Mg alloys have various aspect ratios and are not perfectly spherical. Therefore, it is crucial to develop a physically based precipitation model for Mg alloys that takes into account of the non-spherical morphology of precipitates, which can be achieved through an improved KWN model. High-throughput simulation based on improved KWN modeling offers a powerful tool for optimizing the composition and heat treatment

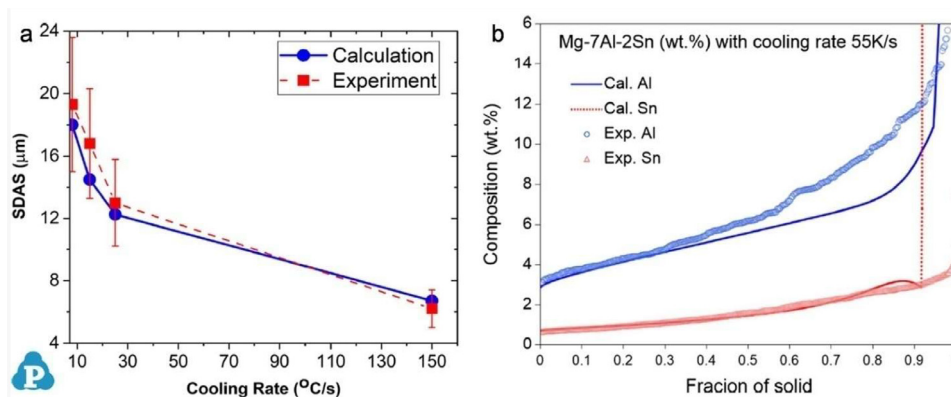


Fig. 27. Simulation solidification microstructure of AT72 alloy: (a) comparison between simulated and measured SDAS of wedge casting AT72 alloy, and (b) comparison between the simulated and measured composition profiles vs fraction of solid [165].

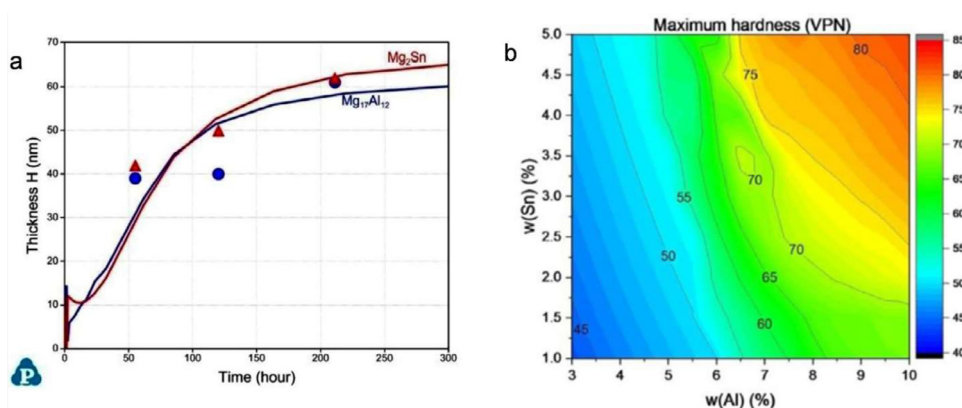


Fig. 28. (a) Simulation of the evolution of the thickness of two kinds of precipitation phases ($Mg_{17}Al_{12}$ and Mg_2Sn) in AT72 alloy aged at 200 °C, and (b) high throughput KWN precipitation simulation of the variation of peak aging hardness with alloying compositions in Mg-Al-Sn systems aged at 200 °C [172].

procedures in precipitation strengthened alloys. A improved CALPHAD-based high-throughput KWN model taking into account of non-spherical precipitates were successfully used to simulate the concurrent precipitation of $Mg_{17}Al_{12}$ and Mg_2Sn in AT72 alloy [172]. Fig. 28(a) shows the comparison of simulated evolution precipitation microstructure as compared with experimental measurements. By coupling with precipitate strengthening models, the high through-put KWN modeling was used to simulate the variation of peak aging response with respect to different Al and Sn compositions as shown in Fig. 28b.

7. Corrosion research

The corrosion susceptibility of Mg and its alloys has long been a barrier to further applications in a variety of fields due to the high electronegativity and poor protective film of Mg. In response, there has been significant work to improve corrosion resistance via alloying and coating solutions. In addition, efforts have been made to leverage the electrochemical activity of Mg as an asset for battery, biomedical, and other applications [173,174], as discussed in Section 2.3.

7.1. Basic corrosion mechanisms

The corrosion mechanism of pure Mg differs from that of all other metals. Under increasing anodic polarization, the cathodic reaction which is the hydrogen evolution for Mg increases. This is a deviation from typical metals where the cathodic reaction rate decreases with anodic polarization. This deviation from expected behavior is called the negative difference effect (NDE) or anomalous hydrogen evolution [175]. To explain this phenomenon, two theories have been proposed: the univalent magnesium theory and the theory of anomalous hydrogen evolution on Mg surface [176–178]. Both can successfully explain the increase in hydrogen evolution. The ability to control the corrosion of Mg will be significantly aided by understanding the underlying mechanisms.

The univalent Mg theory postulates that the production of Mg^+ increases with increasing anodic polarization. A fraction of which reacts chemically to split water to produce excess hydrogen and thus the electrons exchanged are not captured via external circuits. The anomalous hydrogen evolution on the Mg surface argues that the catalytic nature of the Mg surface increases with increasing polarization due to an increase in the exchange current density of the hydrogen evolution

reaction (HER) on the Mg surface. More in-depth descriptions of the development and defenses of univalent Magnesium [177,179,180] and AHE [175,181] theories can be found in the referenced literature.

Experimental evidence for the validation of both theories is difficult as direct observation of the Mg^+ ion is impossible with existing techniques and to date there has not been a complete description of the catalytic sites on the Mg surface. In recent critical review articles [173,182], Antres and Song have discussed both theories and concluded that their univalent Mg^+ theory remains the best explanation for the current experimental observations. Recently, the development of computational modeling with the increasing computational power leads to the possibility of refining the proposed mechanisms which should aid in targeted experimental designs in the future. Fogarty et al. [183] performed a combined molecular dynamics and density functional theory study on the interactions between water and a hydroxylated Mg (1000) surface. This simulation was conducted to study the spontaneous formation of the hydroxylated layer on the bare Mg surface and the interactions of this film with water once formed. They demonstrated the enhanced catalytic nature of the Mg film to the water splitting reaction as well as showed the oxidation of Mg to form univalent Mg^+ ions. The tools developed in that paper will be very beneficial to examining the univalent Mg theory. However, the work has not yet extended to study anodically polarized surfaces nor did the calculations determine if the Mg^+ ion is reacted chemically to form Mg^{2+} as is needed to fully confirm the univalent Mg theory.

Würger et al. [184] studied the mechanism of the hydrogen evolution via density functional theory to determine if the reaction followed a Volmer-Tafel or a Volmer-Heyrovský pathway. The pathway was found to be preferred as it possessed the lower energy barrier to the formation of hydrogen with the Volmer step being rate limiting. They also investigated the energy barrier for a Mg ion to detach from the surface, finding that the removal of Mg^+ ions coordinated with 3 water molecules is less energetically favorable than Mg^{2+} ions coordinated with 6 water molecules. They use this calculated result to argue that Mg^+ ions are not stable in the process of Mg dissolution.

Past critical reviews [182,185] examined the experimental evidence and argued that their univalent Mg^+ theory is the best at explaining the results. There is a lack of recent reviews that argue for the theory of anomalous cathodic hydrogen evolution on Mg surfaces. Understanding the fundamental mechanisms of Mg corrosion is necessary to designing truly corrosion resistant alloys. However, there is still significant work done to design alloys to better accommodate corrosion despite the lack of mechanistic understanding.

7.2. Designing corrosion resistant Mg alloys

Due to the very negative electrochemical potential, Mg is anodic to the majority of secondary phases present in the microstructure and very sensitive to impurity content. Due to this micro galvanic relationship, improving the corrosion re-

sistance of Mg alloys conflicts with efforts to produce higher mechanical properties via alloying. The Mg_2Ca phase is an exception to this rule with recent studies showing its anodic relationship to the α -Mg matrix via highly local corrosion techniques [186–188]. This has resulted in extensive work on Mg-Ca binary and Ca-containing alloys as an avenue to corrosion resistant alloys. This will be discussed in more detail in a further section.

Reducing corrosion susceptibility is commonly approached from two directions: 1) reducing the cathodic initiation from secondary phases; or 2) improving stability and protectiveness of the corrosion film. Microalloying of Ca and RE additions have shown considerable progress to create more corrosion resistant alloys. However, to date, there is no truly “stainless” Mg alloy system as none show a truly passive film but a few alloys have achieved slower corrosion than the intrinsic corrosion rate of pure Mg which is 0.3 mm/yr in 3.5% NaCl [189,190]. Impurity management and micro alloying have successfully reduced the corrosion rate below the intrinsic rate. Further testing is needed to see how to utilize these discoveries to discover a truly corrosion resistant Mg alloy.

7.3. Iron impurity tolerance

The importance of purity of Mg corrosion has long been understood with Hanawalt outlining the tolerance limits of common impurities in 1942 [191]. Fe, Ni, Cr, and Cu are the most studied impurities around corrosion control due to the large galvanic potential relative to Mg as well as their prevalence in the ore and ability to be introduced during refining [192]. Excess impurities will result in extensive local corrosion around impurity-phases and regions of high impurity segregation. Therefore, determining strict safe limits of the impurities is important to ensure consistent and predictable degradation behavior.

The use of Fe-based tools and equipment results in Fe being picked up throughout alloy production and processing. Fortunately, Mg can tolerate a low Fe content before the corrosion rate is accelerated. However, the specific tolerance limit and mechanisms are still being explored. Hanawalt’s original study shows a limit of 170 ppm in otherwise high purity Mg which is above the solid solution limit of 5 ppm [191]. Recently, studies show both higher [193] and lower [194–196] tolerances in high purity Mg. This inconsistency is because the acceleration of corrosion depending on more than Fe concentration. Alloying elements [197–199], casting conditions [198], thermal processing [196,200,201], and interactions with other impurities like Si [202] and In [200] all play a nonnegligible role in determining the tolerance limit. However, the current research is concentrated around pure Mg and Al containing Mg alloys. More work is needed to understand iron tolerance in other alloy systems.

7.4. Micro-alloying additions

Micro-alloying is used to modify microstructures, surface films, or impurity effects to improve the corrosion resistance

of Mg alloys. Ca has gained attention as a potential alloying element to control corrosion in Mg as it is one of the few metals more electrochemically active than Mg. Micro addition of Ca have shown improved corrosion resistance in Mg-Ca binary alloys as well as in existing Mg alloys [203–206]. In Mg-Ca binary alloys, Ca is beneficial in small amounts with many studies finding samples with the lowest concentration of Ca showing more uniform and slower corrosion than pure Mg or samples with more Ca [207–210]. The extra Ca precipitates into more Mg₂Ca phase at the grain boundaries, resulting in more mass loss during immersion testing [207]. Deng et al. investigated Mg micro-alloyed with Ca between 0.05–0.15% and showed that Mg with 0.15% Ca had the best corrosion performance with a corrosion rate of ~0.1 mm/yr after 7 days immersion in 3.5% NaCl, which was even lower than ~0.3 mm/yr measured on the high purity Mg [203]. The improved corrosion resistance was determined to be a result of Ca restricting the kinetics of the water reduction reaction and producing a dense thin surface film quickly once immersed. They also discussed the potential role of Ca in limiting the ability of Fe impurities to precipitate. They argued that this is due to Si, which would normally help with Fe precipitation, is used to form small Mg-Ca-Si phases or clusters. Deng et al. continued this work by exploring the effects of thermal mechanical processing on the Mg-0.15Ca alloy and found significantly accelerated corrosion after heat treatment, rolling, or extrusion [200]. This was the result of Fe precipitation during processing despite only having 16 ppm Fe. This significantly hinders Mg-Ca alloys usability as it is restricted to as cast condition. Additional micro-alloying of Ge, Sn, and In were attempted in the same work with only In able to prevent significant corrosion after thermomechanical processing. They speculate this is a result of In modifying the solubility of Fe in the α -Mg matrix.

7.5. Magnesium-rare earth (RE) alloys

In Mg alloys, RE elements have been used to improve both corrosion resistance and mechanical performance simultaneously [211]. The uniqueness of RE is their similar electrochemical potential to Mg so that precipitation of RE-containing phases can strengthen the material without significant cathodic acceleration as seen with other phases like those containing Al or Zn [212–214]. Additionally, Mg-RE alloys have shown potential to significantly modify the corrosion film such that it becomes more protective. Recently, Zhu et al. have demonstrated the ability of Mg-11Y-1Al to spontaneously generate a dense film of Y₂O₃, MgO, and AlO₃ [190]. This was found to be the result of Al precipitating onto the surface as Al(OH)₃ and acting as a nucleation site for both Mg and Y containing hydrides. Without Al, the Mg-11Y alloy possessed little Y in the film resulting in worse corrosion performance compared to AZ91D and commercially pure (CP) Mg. Using multiple elements to aid in the formation of a truly passive film warrants further study especially if it can produce similar improvements with less-RE or cheaper RE than Y.

The economic and environmental cost of increasing RE usage globally combined with the higher density of RE containing alloys has resulted in extensive work to use lean-RE additions to achieve similar improvements [115,215,216]. Simultaneous exploitation of reduced cathodic potential in secondary phases and element assisted protective film formation is showing great promise to create truly corrosion resistant “stainless” Mg alloys.

8. Summary and future outlook

As summarized in this article, it is our belief that Mg as a material class is presently at a crossroads, facing 1) enormous technical and sustainability challenges as an industrial metal for mass production; and 2) significant opportunities but substantial road blocks as a technology metal for emerging applications in biomedical devices and energy systems. The following strategies are suggested:

- 1) Non/low-carbon production of primary Mg: Current Pidgeon process production needs to be dramatically improved or gradually phased out due to its inherent CO₂ emissions. More production of Mg is needed using electrolytical or non-carbon thermal reduction processes.
- 2) Increased end-of-life (EOL) recycling of Mg components: It is important to increase sorting and collecting EOL Mg scrap for recycling to produce secondary Mg alloys to achieve material circularity in Mg.
- 3) Total life cycle assessment (LCA) for Mg production: It is suggested that an international LCA for Mg production including major Mg producing countries be conducted by a neutral organization/committee to provide creditable data for end-users to access the carbon footprint and energy consumption in various steps of Mg primary production and downstream manufacturing. Such information will build confidence of Mg as an important industrial metal.
- 4) Corrosion-resistant (“stainless”) Mg alloys: Fundamental research on Mg corrosion mechanisms has generated important guidance for developing corrosion-resistant Mg alloys. Current research has shown promises of using Ca and RE alloying to substantially improve the corrosion resistance of Mg alloys. Future efforts are needed to optimize and scale up these materials for truly *stainless* Mg alloys for industrial applications.
- 5) Flame-resistant Mg alloy development: Flame resistance is a critical requirement for aerospace applications including interior (seat and luggage compartment) components. Ca and RE elements have been found to increase the ignition temperature of Mg alloys, and new Mg alloys should be certified for aerospace applications.
- 6) Alloy development for high thermal and electric conductivity: Applications in electric, electronics and consumer products often require conductivity of heat and electricity for their functional (in addition to mechanical) performance. New Mg alloys balancing mechanical

properties and conductivity are needed for these applications.

- 7) Mg-based advanced material development: Emerging materials including metal matrix composites (with micro- and nano-scale reinforcements), multicomponent concentrated (high or medium entropy) alloys, functionally gradient materials should be investigated to make Mg both an industry and a technology metal for the future.
- 8) Mega-casting development: One of the new developments for aluminum applications is the large thin-wall die casting (mega/giga castings) for automotive body structures especially for electric vehicles. With better castability in terms of fluidity and thin-wall capability of Mg vs. Al alloys, it is expected that Mg mega-castings will be used in these applications, provided that joining and corrosion issues can be addressed via design and coating/isolation measures.
- 9) Room temperature (RT) Mg forming: The room-temperature formability of Mg alloys with HCP crystalline structure can be significantly improved via micro-alloying with Ca or Ce which modifies texture and refine grain structure. New Mg sheet and extrusion alloys with comparable RT formability of Al sheet alloys offer opportunities for Mg sheet components in automotive, aerospace and electronics industries.
- 10) Additive manufacturing (AM): AM is emerging processes for making low-volume Mg products from CAD design to finished products with no hard tooling needed, especially for personalized medical devices. It is still challenging to produce high-quality Mg powder in a safe and robust process. Thus, wire-based AM processes have advantages over powder-based processes. Also, binder-jetting process is faster and safer than fusion-based AM process, despite the need of subsequent sintering process for binder-jetting printed parts.
- 11) Mg-ion battery development: Mg-ion battery is a promising new technology which could replace Li-ion batteries, due to the lower cost and a more abundant supply of Mg than Li metal. Major challenges for Mg-ion battery technology include its electrolyte and cathode development. Mg anode can react with many organic electrolytes to form ionic insulating passivation films resulting in irreversible plating and stripping, which could be mitigated by new Mg alloy anode and coating technology.
- 12) Hydrogen storage: Mg hydride has a higher gravimetry hydrogen capacity and lower cost compared to other hydride-forming metals such as Li. However, its sluggish hydrogenation/dehydrogenation kinetics requires higher operating temperatures, which need to be resolved. New Mg hydride chemistry and processing techniques are expected to improve the kinetics of hydrogen absorption/desorption and reduce the operation temperatures.

Going forward, with increasing global research and development efforts on Mg alloys, process innovations and product development, Mg can grow both as an industrial metal for lightweighting applications in many sectors, and as a technology metal for emerging biomedical and energy applications.

Declaration of competing interest

Alan Luo is an associate editor for Journal of Magnesium and Alloys and was not involved in the editorial review or the decision to publish this article. All authors declare that there are no competing interests.

CRediT authorship contribution statement

Jianyue Zhang: Writing – original draft. **Jiashi Miao:** Writing – original draft. **Nagasivamuni Balasubramani:** Writing – original draft. **Dae Hyun Cho:** Writing – original draft. **Thomas Avey:** Writing – original draft. **Chia-Yu Chang:** Writing – original draft. **Alan A. Luo:** Conceptualization, Supervision, Writing – original draft, Writing – review & editing.

Acknowledgements

The authors are grateful to the support and collaboration of numerous colleagues and students at The Ohio State University (OSU), as well as industrial partners including General Motors (GM), Meridian and Terves. The authors acknowledge the financial support from the United States National Science Foundation and Department of Energy.

References

- [1] L. Bray, Magnesium Metal, U.S. Geological Survey, Mineral Commodity Summaries, n.d. <http://pubs.er.usgs.gov/publication/mcs2023>.
- [2] S. Ehrenberger, IMA LCA Study 30 (2020).
- [3] A. Clark, Global Primary Mg Production Supply Demand 2020, Presentation at IMA 2021, 2021 August.
- [4] M.F. Ashby, Materials and the Environment, 2009.
- [5] G. Bhutada, Vis. Capital. (2021) 1–10 <https://www.visualcapitalist.com/all-the-metals-we-mined-in-one-visualization/>.
- [6] R.E. Brown, Present. Mater. Sci. Technol. Conf. Pittsburgh, 2008 Oct. 5–9.
- [7] B.R. Powell, P.E. Krajewski, A.A. Luo, LTD (2020), doi:10.1016/B978-0-12-818712-8.00004-5.
- [8] B. Liu, J. Yang, X. Zhang, Q. Yang, J. Zhang, X. Li, J. Magnes. Alloy. 11 (2023) 15–47, doi:10.1016/j.jma.2022.12.015.
- [9] Ducker Carlisle, Light Vehicle Aluminum Content and Outlook Study, 2023 April.
- [10] T.R. Marker, Evaluating the Flammability of Various Magnesium Alloys During Laboratory-and Full-Scale Aircraft Fire Tests, U.S. Department of Transportation Federal Aviation Administration Report, DOT/FAA/AR-11/3, 2013 January.
- [11] AS8049B: Performance Standard for Seats in Civil Rotorcraft, Transport Aircraft, and General Aviation Aircraft, 2015 August 14.
- [12] Aerospace Magnesium Alloys Market, Global Outlook and Forecast 2023–2030, <https://www.24chemicalresearch.com/download-sample/236909/global-aerospace-magnesium-alloys-forecast-market-2023-2030-559/>.

- [13] S. Sankaranarayanan, M. Gupta, *Mater. Today Proc.* 39 (2020) 311–316, doi:10.1016/j.matpr.2020.07.220.
- [14] V.V. Ramalingam, P. Ramasamy, M. Das Kovukkal, G. Myilsamy, *Met. Mater. Int.* 26 (2020) 409–430, doi:10.1007/s12540-019-00346-8.
- [15] K. V. N. Kumar B, S. Kumar S, V. M, *Addit. Manuf.* 55 (2022) 102802, doi:10.1016/j.addma.2022.102802.
- [16] G. Chandra, A. Pandey, *IRBM* 43 (2022) 229–249, doi:10.1016/j.irbm.2020.06.003.
- [17] F. Witte, *Acta Biomater.* 6 (2010) 1680–1692, doi:10.1016/j.actbio.2010.02.028.
- [18] J. Chen, Y. Xu, S.K. Kolawole, J. Wang, X. Su, L. Tan, K. Yang, *Materials* 15 (2022), doi:10.3390/ma15145031.
- [19] Z.Q. Zhang, Y.X. Yang, J.A. Li, R.C. Zeng, S.K. Guan, *Bioact. Mater.* 6 (2021) 4729–4757, doi:10.1016/j.bioactmat.2021.04.044.
- [20] R. Zan, S. Shen, Y. Huang, H. Yu, Y. Liu, S. Yang, B. Zheng, Z. Gong, W. Wang, X. Zhang, T. Suo, H. Liu, *Smart Mater. Med.* 4 (2023) 468–479, doi:10.1016/j.smaim.2023.01.002.
- [21] P. Sekar, N. S, V. Desai, *J. Magnes. Alloy.* 9 (2021) 1147–1163, doi:10.1016/j.jma.2020.11.001.
- [22] H. Waizy, J. Diekmann, A. Weizbauer, J. Reifenrath, I. Bartsch, V. Neubert, R. Schavan, H. Windhagen, *J. Biomater. Appl.* 28 (2014) 667–675, doi:10.1177/0885328212472215.
- [23] J.W. Lee, H.S. Han, K.J. Han, J. Park, H. Jeon, M.R. Ok, H.K. Seok, J.P. Ahn, K.E. Lee, D.H. Lee, S.J. Yang, S.Y. Cho, P.R. Cha, H. Kwon, T.H. Nam, J.H. Lo Han, H.J. Rho, K.S. Lee, Y.C. Kim, D. Mantovani, *Proc. Natl. Acad. Sci. U.S.A.* 113 (2016) 716–721, doi:10.1073/pnas.1518238113.
- [24] P. Rider, Ž.P. Kačarević, A. Elad, D. Tadic, D. Rothamel, G. Sauer, F. Bornert, P. Windisch, D.B. Hangyási, B. Molnar, E. Bortel, B. Hesse, F. Witte, *Bioact. Mater.* 14 (2022) 152–168, doi:10.1016/j.bioactmat.2021.11.018.
- [25] D. Li, D. Zhang, Q. Yuan, L. Liu, H. Li, L. Xiong, X. Guo, Y. Yan, K. Yu, Y. Dai, T. Xiao, Y. Li, C. Wen, *Acta Biomater.* 141 (2022) 454–465, doi:10.1016/j.actbio.2021.12.032.
- [26] P. Makkar, H.J. Kang, A.R. Padalhin, O. Faruq, B.T. Lee, *Appl. Surf. Sci.* 510 (2020) 145333, doi:10.1016/j.apsusc.2020.145333.
- [27] G. Li, L. Zhang, L. Wang, G. Yuan, K. Dai, J. Pei, Y. Hao, *Acta Biomater.* 65 (2018) 486–500, doi:10.1016/j.actbio.2017.10.033.
- [28] R. Deivanayagam, B.J. Ingram, R. Shahbazian-Yassar, *Energy Storage Mater.* 21 (2019) 136–153, doi:10.1016/j.ensm.2019.05.028.
- [29] M. Song, L. Zhang, F. Wu, H. Zhang, H. Zhao, L. Chen, H. Li, *J. Mater. Sci. Technol.* 149 (2023) 99–111, doi:10.1016/j.jmst.2022.11.032.
- [30] Y. Sun, C. Shen, Q. Lai, W. Liu, D.W. Wang, K.F. Aguey-Zinsou, *Energy Storage Mater.* 10 (2018) 168–198, doi:10.1016/j.ensm.2017.01.010.
- [31] M. Simanullang, L. Prost, *Int. J. Hydrogen Energy* 47 (2022) 29808–29846, doi:10.1016/j.ijhydene.2022.06.301.
- [32] S. Ehrenberger, H. Diering, H.E. Friedrich, in: *Life Cycle Assessment of Magnesium Components in Vehicle Construction*, German Aerospace Centre e.V. Institute of Vehicle Concepts, Stuttgart, Germany, 2013, pp. 1–109.
- [33] J. Søreide, (2021) 1–7. https://www.hydro.com/en/about-hydro/stories-by-hydro/do-you-see-what-we-see-not-all-recycled-aluminium-is-equal/?utm_campaign=greener_2021&utm_medium&link&utm_source&climate-action&utm_term=position-paper&utm_content=paid.
- [34] A.A. Luo, *J. Magnes. Alloy.* 1 (2013) 2–22, doi:10.1016/j.jma.2013.02.002.
- [35] A.A. Luo, *Int. Mater. Rev.* 49 (2004) 13–30, doi:10.1179/095066004225010497.
- [36] C. Su, D. Li, J. Wang, R. Shi, A.A. Luo, X. Zeng, Z. Lin, J. Chen, *Mater. Sci. Eng. A.* 773 (2020) 138870, doi:10.1016/j.msea.2019.138870.
- [37] M.M. Avedesian, H. Baker, *ASM Specialty handbook: Magnesium and Magnesium Alloys*, ASM international, 1999.
- [38] A.A. Luo, P. Fu, L. Peng, X. Kang, Z. Li, T. Zhu, *Metall. Mater. Trans. A Phys. Metall. Mater. Sci.* 43 (2012) 360–368, doi:10.1007/s11661-011-0820-y.
- [39] A.D. Klarner, J. Miao, W. Sun, A.A. Luo, X. Zeng, *Metall. Mater. Trans. A Phys. Metall. Mater. Sci.* 50 (2019) 1522–1533, doi:10.1007/s11661-018-5061-x.
- [40] Z. Li, A.A. Luo, Q. Wang, H. Zou, J. Dai, L. Peng, *J. Magnes. Alloy.* 5 (2017) 1–12, doi:10.1016/j.jma.2017.03.001.
- [41] Z. Li, Q. Wang, A.A. Luo, J. Dai, H. Zou, L. Peng, *J. Mater. Sci. Technol.* 34 (2018) 2091–2099, doi:10.1016/j.jmst.2018.05.001.
- [42] D.H. Cho, T. Avey, K.H. Nam, D. Dean, A.A. Luo, *Acta Biomater.* 150 (2022) 442–455, doi:10.1016/j.actbio.2022.07.040.
- [43] J. Pan, L. Peng, P. Fu, H. Zhang, J. Miao, H. Yue, A.A. Luo, *Mater. Sci. Eng. A* 754 (2019) 246–257, doi:10.1016/j.msea.2019.03.063.
- [44] J. Zhang, P. Peng, A.A. Luo, J. She, A. Tang, F. Pan, *Mater. Sci. Eng. A.* 829 (2022) 142143, doi:10.1016/j.msea.2021.142143.
- [45] A.A. Luo, A.K. Sachdev, *Metall. Mater. Trans. A Phys. Metall. Mater. Sci.* 38 (2007) 1184–1192, doi:10.1007/s11661-007-9129-2.
- [46] R.K. Mishra, A.K. Gupta, P.R. Rao, A.K. Sachdev, A.M. Kumar, A.A. Luo, *Essent. Readings Magnes. Technol.* (2016) 363–368.
- [47] R.K. Sabat, A.P. Brahme, R.K. Mishra, K. Inal, S. Suwas, *Acta Mater.* 161 (2018) 246–257, doi:10.1016/j.actamat.2018.09.023.
- [48] A.A. Luo, R.K. Mishra, A.K. Sachdev, *Scr. Mater.* 64 (2011) 410–413, doi:10.1016/j.scriptamat.2010.10.045.
- [49] H. Pan, G. Qin, Y. Huang, Y. Ren, X. Sha, X. Han, Z.Q. Liu, C. Li, X. Wu, H. Chen, C. He, L. Chai, Y. Wang, J. feng Nie, *Acta Mater.* 149 (2018) 350–363, doi:10.1016/j.actamat.2018.03.002.
- [50] Z.T. Li, X.G. Qiao, C. Xu, S. Kamado, M.Y. Zheng, A.A. Luo, *J. Alloys Compd.* 792 (2019) 130–141, doi:10.1016/j.jallcom.2019.03.319.
- [51] A. Zhang, R. Kang, L. Wu, H. Pan, H. Xie, Q. Huang, Y. Liu, Z. Ai, L. Ma, Y. Ren, G. Qin, *Mater. Sci. Eng. A* 754 (2019) 269–274, doi:10.1016/j.msea.2019.03.095.
- [52] M. Li, D. Xie, J. Li, H. Xie, Q. Huang, H. Pan, G. Qin, *Mater. Charact.* 175 (2021) 111049, doi:10.1016/j.matchar.2021.111049.
- [53] Z. Zeng, N. Stanford, C.H.J. Davies, J.F. Nie, N. Birbilis, *Int. Mater. Rev.* 64 (2019) 27–62, doi:10.1080/09506608.2017.1421439.
- [54] P. Peng, A. Tang, B. Wang, S. Zhou, J. She, J. Zhang, F. Pan, *J. Mater. Res. Technol.* 15 (2021) 1252–1265, doi:10.1016/j.jmrt.2021.08.133.
- [55] P. Peng, J. She, A. Tang, J. Zhang, K. Song, Q. Yang, F. Pan, *J. Alloys Compd.* 890 (2022) 161789, doi:10.1016/j.jallcom.2021.161789.
- [56] C.C. Li, Z.H. Xia, X.G. Qiao, I.S. Golovin, M.Y. Zheng, *Mater. Sci. Eng. A* 869 (2023), doi:10.1016/j.msea.2022.144508.
- [57] H. Somekawa, D.A. Basha, A. Singh, *Mater. Sci. Eng. A* 730 (2018) 355–362, doi:10.1016/j.msea.2018.06.015.
- [58] P. Peng, J. She, A. Tang, J. Zhang, S. Zhou, M. Rashad, J. Kim, A.A. Luo, F. Pan, *Mater. Sci. Eng. A* 859 (2022) 144229, doi:10.1016/j.msea.2022.144229.
- [59] P. Peng, X. He, J. She, A. Tang, M. Rashad, S. Zhou, G. Zhang, X. Mi, F. Pan, *Mater. Sci. Eng. A* 766 (2019) 138332, doi:10.1016/j.msea.2019.138332.
- [60] J. She, P. Peng, L. Xiao, A.T. Tang, Y. Wang, F.S. Pan, *Mater. Sci. Eng. A.* 765 (2019) 138203, doi:10.1016/j.msea.2019.138203.
- [61] H. Liao, J. Kim, T. Liu, A. Tang, J. She, P. Peng, F. Pan, *Mater. Sci. Eng. A* 754 (2019) 778–785, doi:10.1016/j.msea.2019.02.021.
- [62] S. Zhou, T. Liu, A. Tang, H. Shi, T. Chen, P. Peng, J. Zhang, J. She, F. Pan, *J. Mater. Res. Technol.* 20 (2022) 3522–3536, doi:10.1016/j.jmrt.2022.08.091.
- [63] P. Peng, J. She, Q. Yang, S. Long, A. Tang, J. Zhang, Q. Dai, F. Pan, *J. Alloys Compd.* 935 (2023) 168008, doi:10.1016/j.jallcom.2022.168008.
- [64] J. Zhang, P. Peng, Q. Yang, A.A. Luo, *J. Magnes. Alloy.* (2023), doi:10.1016/j.jma.2022.12.012.
- [65] G. Zhu, L. Wang, H. Zhou, J. Wang, Y. Shen, P. Tu, H. Zhu, W. Liu, P. Jin, X. Zeng, *Int. J. Plast.* 120 (2019) 164–179, doi:10.1016/j.iplas.2019.04.020.
- [66] J. Wang, Y. Chen, Z. Chen, J. Llorca, X. Zeng, *Acta Mater.* 217 (2021) 117151, doi:10.1016/j.actamat.2021.117151.
- [67] H. Ding, X. Shi, Y. Wang, G. Cheng, S. Kamado, *Mater. Sci. Eng. A* 645 (2015) 196–204, doi:10.1016/j.msea.2015.08.025.

- [68] Z.H. Li, T.T. Sasaki, M.Z. Bian, T. Nakata, Y. Yoshida, N. Kawabe, S. Kamado, K. Hono, *J. Alloys Compd.* 847 (2020) 1–11, doi:10.1016/j.jallcom.2020.156347.
- [69] R. Shi, J. Miao, A.A. Luo, *Scr. Mater.* 171 (2019) 92–97, doi:10.1016/j.scriptamat.2019.06.027.
- [70] J.F. Nie, *Metall. Mater. Trans. A Phys. Metall. Mater. Sci.* 43 (2012) 3891–3939, doi:10.1007/s11661-012-1217-2.
- [71] R. Shi, J. Miao, T. Avey, A.A. Luo, *Sci. Rep.* 10 (2020) 18–23, doi:10.1038/s41598-020-67161-9.
- [72] A.A. Luo, R. Shi, J. Miao, T. Avey, *JOM* 73 (2021) 1403–1418, doi:10.1007/s11837-021-04616-y.
- [73] A. Jones, J.H. Lennon, R.R. Nash, W.H. Chang, E.G. MacPeck, *Magnesium Alloy Research Studies*, 1952.
- [74] Y.C. Lee, A.K. Dahle, D.H. St John, *Essent. Read. Magnes. Technol.* (2014) 247–254 9781118858, doi:10.1002/9781118859803.ch41.
- [75] B. Nagasivamuni, G. Wang, D.H. StJohn, M.S. Dargusch, *J. Cryst. Growth* 512 (2019) 20–32, doi:10.1016/j.jcrysgro.2019.02.004.
- [76] N. Balasubramani, G. Wang, M.A. Easton, D.H. StJohn, M.S. Dargusch, *J. Magnes. Alloy.* 9 (2021) 829–839, doi:10.1016/j.jma.2020.08.006.
- [77] D.H. Stjohn, M.A. Easton, M. Qian, J.A. Taylor, *Metall. Mater. Trans. A Phys. Metall. Mater. Sci.* 44 (2013) 2935–2949, doi:10.1007/s11661-012-1513-x.
- [78] D.H. StJohn, P. Cao, M. Qian, M.A. Easton, *A Brief History of the Development of Grain Refinement Technology for Cast Magnesium Alloys*, 2013, doi:10.1002/9781118805497.
- [79] G.S. Peng, Y. Wang, Z. Fan, *Metall. Mater. Trans. A Phys. Metall. Mater. Sci.* 49 (2018) 2182–2192, doi:10.1007/s11661-018-4594-3.
- [80] X. Tong, G. Wu, M.A. Easton, M. Sun, D.H. StJohn, R. Jiang, F. Qi, *Scr. Mater.* 215 (2022) 114700, doi:10.1016/j.scriptamat.2022.114700.
- [81] E. Karakulak, *J. Magnes. Alloy.* 7 (2019) 355–369, doi:10.1016/j.jma.2019.05.001.
- [82] Y. Wang, X. Zeng, W. Ding, A.A. Luo, A.K. Sachdev, *Metall. Mater. Trans. A Phys. Metall. Mater. Sci.* 38 (2007) 1358–1366, doi:10.1007/s11661-007-9215-5.
- [83] A. Luo, *Can. Metall. Q.* 35 (1996) 375–383.
- [84] J. Zhang, G. Zhou, B. Jiang, A. Luo, X. Zhao, A. Tang, F. Pan, *Metals* 11 (2021), doi:10.3390/met11111722.
- [85] Y. Huang, J. Gu, S. You, K. Ulrich Kainer, N. Hort, *IOP Conf. Ser. Mater. Sci. Eng.* 529 (2019), doi:10.1088/1757-899X/529/1/012049.
- [86] D.H. Stjohn, M. Qian, M.A. Easton, P. Cao, *Acta Mater.* 59 (2011) 4907–4921, doi:10.1016/j.actamat.2011.04.035.
- [87] D.H. StJohn, A. Prasad, M.A. Easton, M. Qian, *Metall. Mater. Trans. A Phys. Metall. Mater. Sci.* 46 (2015) 4868–4885, doi:10.1007/s11661-015-2960-y.
- [88] Z. Fan, F. Gao, Y. Wang, S.H. Wang, J.B. Patel, *J. Magnes. Alloy.* 10 (2022) 2919–2945, doi:10.1016/j.jma.2022.10.006.
- [89] W. Fan, Y. Bai, J. Li, G. Li, H. Hao, *J. Mater. Eng. Perform.* 32 (2023) 761–772, doi:10.1007/s11665-022-07110-x.
- [90] N. Balasubramani, J. Venezuela, D. StJohn, G. Wang, M. Dargusch, *J. Mater. Sci. Technol.* 144 (2023) 243–265, doi:10.1016/j.jmst.2022.09.067.
- [91] D. Gao, Z. Li, Q. Han, Q. Zhai, *Mater. Sci. Eng. A* 502 (2009) 2–5, doi:10.1016/j.msea.2008.12.005.
- [92] H. Xu, X. Jian, T.T. Meek, Q. Han, *Mater. Lett.* 58 (2004) 3669–3673, doi:10.1016/j.matlet.2004.02.055.
- [93] Q. Han, *Metall. Mater. Trans. B Process Metall. Mater. Process. Sci.* 46 (2015) 1603–1614, doi:10.1007/s11663-014-0266-x.
- [94] G.G. Wang, J.P. Weiler, *J. Magnes. Alloy.* 11 (2022) 78–87, doi:10.1016/j.jma.2022.10.001.
- [95] N. Trometer, L.A. Godlewski, E. Prabhu, M. Schopen, A.A. Luo, *Int. J. Met.* (2023) 1–17.
- [96] G.G. Wang, K. Mackenzie, C. Sweet, J.T. Carter, J.C. O’Kane, S.A. Resch, A.K. Sachdev, A.A. Luo, *SAE Int. J. Mater. Manuf.* 13 (2020) 199–208, doi:10.4271/05-13-03-0016.
- [97] N. Srivastava, M. Anas, *Mater. Today Proc.* 26 (2019) 1914–1920, doi:10.1016/j.matpr.2020.02.419.
- [98] M.R. Ghomashchi, A. Vikhrov, *J. Mater. Process. Technol.* 101 (2000) 1–9, doi:10.1016/S0924-0136(99)00291-5.
- [99] A.S. Marodkar, H. Patil, J. Chavhan, H. Borkar, *Mater. Today Proc.* (2023), doi:10.1016/j.matpr.2023.03.053.
- [100] H. Patil, A. Marodkar, A. Ghosh, H. Borkar, *Mater. Today Proc.* (2023), doi:10.1016/j.matpr.2023.03.056.
- [101] C. Wang, H. Li, Q. He, J. Wu, G. Wu, W. Ding, *Mater. Charact.* 184 (2022) 111658, doi:10.1016/j.matchar.2021.111658.
- [102] R. Xiao, W. Liu, G. Wu, L. Zhang, B. Liu, W. Ding, *Trans. Nonferrous Met. Soc. China* 31 (2021) 1572–1586, doi:10.1016/S1003-6326(21)65599-1.
- [103] D.H. Cho, B.W. Lee, J.Y. Park, K.M. Cho, I.M. Park, *J. Alloys Compd.* 695 (2017) 1166–1174, doi:10.1016/j.jallcom.2016.10.244.
- [104] P. Peng, J. She, A. Tang, J. Zhang, S. Zhou, X. Xiong, F. Pan, *Mater. Sci. Eng. A* 764 (2019) 138144, doi:10.1016/j.msea.2019.138144.
- [105] P. Peng, K. Zhang, J. She, A. Tang, J. Zhang, K. Song, Q. Yang, F. Pan, *J. Alloys Compd.* (2020) 157958, doi:10.1016/j.jallcom.2020.157958.
- [106] J. He, B. Jiang, J. Xu, J. Zhang, X. Yu, B. Liu, F. Pan, *J. Alloys Compd.* 723 (2017) 213–224, doi:10.1016/j.jallcom.2017.06.269.
- [107] J. He, B. Jiang, J. Zhang, Q. Xiang, X. Xia, F. Pan, *Mater. Sci. Eng. A* 647 (2015) 216–221, doi:10.1016/j.msea.2015.09.002.
- [108] Q. Yang, B. Jiang, B. Song, Z. Yu, D. He, Y. Chai, J. Zhang, F. Pan, *J. Magnes. Alloy.* 10 (2022) 411–422, doi:10.1016/j.jma.2020.08.005.
- [109] Y.T. Zhu, T.G. Langdon, *JOM* 56 (2004) 58–63, doi:10.1007/s11837-004-0294-0.
- [110] J. Zhang, Y. Jian, X. Zhao, D. Meng, F. Pan, Q. Han, *J. Magnes. Alloy.* (2020), doi:10.1016/j.jma.2020.11.012.
- [111] J. Zhang, P. Peng, J. She, B. Jiang, A. Tang, F. Pan, Q. Han, *Surf. Coatings Technol.* 396 (2020) 125968, doi:10.1016/j.surfcoat.2020.125968.
- [112] Y. Yuan, A. Ma, X. Gou, J. Jiang, F. Lu, D. Song, Y. Zhu, *Mater. Sci. Eng. A* 630 (2015) 45–50, doi:10.1016/j.msea.2015.02.004.
- [113] Y.V.R.K. Prasad, H.L. Gegel, S.M. Doraivelu, J.C. Malas, J.T. Morgan, K.A. Lark, D.R. Barker, *Metall. Trans. A* 15 (1984) 1883–1892, doi:10.1007/BF02664902.
- [114] S.C. Sutton, A.A. Luo, *J. Magnes. Alloy.* 8 (2020) 111–126, doi:10.1016/j.jma.2019.11.007.
- [115] T. Avey, J. Miao, J. Caris, A.K. Sachdev, A. Luo, in: *World, Springer Nature Switzerland, Cham*, 2023, pp. 189–195. file:///Users/alex.neumann/Documents/Mendeley Desktop/Edited by Edited by World/[Darren Swanson].Creating Adaptive Policies_A_Gui(BookSee.org).pdf.
- [116] A. Vafadar, F. Guzzomi, A. Rassau, K. Hayward, *Appl. Sci.* 11 (2021) 1–33, doi:10.3390/app11031213.
- [117] S. Cooke, K. Ahmadi, S. Willerth, R. Herring, *J. Manuf. Process.* 57 (2020) 978–1003, doi:10.1016/j.jmapro.2020.07.025.
- [118] Y. Qin, P. Wen, H. Guo, D. Xia, Y. Zheng, L. Jauer, R. Poprawe, M. Voshage, J.H. Schleifenbaum, *Acta Biomater.* 98 (2019) 3–22, doi:10.1016/j.actbio.2019.04.046.
- [119] R. Kumar, M. Kumar, J.S. Chohan, *J. Manuf. Process.* 64 (2021) 828–850, doi:10.1016/j.jmapro.2021.02.022.
- [120] Z. Zeng, M. Salehi, A. Kopp, S. Xu, M. Esmaily, N. Birbilis, *J. Magnes. Alloy.* 10 (2022) 1511–1541, doi:10.1016/j.jma.2022.03.001.
- [121] R. Allavikutty, P. Gupta, T.S. Santra, J. Rengaswamy, *Curr. Opin. Biomed. Eng.* 18 (2021) 100276, doi:10.1016/j.cobme.2021.100276.
- [122] R. Karunakaran, S. Ortgies, A. Tamayol, F. Bobaru, M.P. Sealy, *Bioact. Mater.* 5 (2020) 44–54, doi:10.1016/j.bioactmat.2019.12.004.
- [123] C.C. Ng, M.M. Savalani, H.C. Man, I. Gibson, *Virtual Phys. Prototyp.* 5 (2010) 13–19, doi:10.1080/17452751003718629.
- [124] K. Li, C. Ji, S. Bai, B. Jiang, F. Pan, *J. Mater. Sci. Technol.* 154 (2023) 65–93, doi:10.1016/j.jmst.2022.12.053.
- [125] C.C. Ng, M.M. Savalani, M.L. Lau, H.C. Man, *Appl. Surf. Sci.* 257 (2011) 7447–7454, doi:10.1016/j.apsusc.2011.03.004.
- [126] M.H. Nasab, D. Gastaldi, N.F. Lecis, M. Vedani, *Addit. Manuf.* 24 (2018) 373–377, doi:10.1016/j.addma.2018.10.011.
- [127] T. DeRoy, H.L. Wei, J.S. Zuback, T. Mukherjee, J.W. Elmer, J.O. Milewski, A.M. Beese, A. Wilson-Heid, A. De, W. Zhang, *Prog. Mater. Sci.* 92 (2018) 112–224, doi:10.1016/j.pmatsci.2017.10.001.

- [128] M. Ahmadi, S.A.A.B. Tabary, D. Rahmatyabadi, M.S. Ebrahimi, K. Abrinia, R. Hashemi, J. Mater. Res. Technol. 19 (2022) 1537–1562, doi:10.1016/j.jmrt.2022.05.102.
- [129] J. Liu, P. Wen, Mater. Des. 215 (2022) 110505, doi:10.1016/j.matdes.2022.110505.
- [130] R. Motallebi, Z. Savaedi, H. Mirzadeh, J. Mater. Res. Technol. 20 (2022) 1873–1892, doi:10.1016/j.jmrt.2022.07.154.
- [131] M.G. Fard, F. Sharifianjazi, S.S. Kazemi, H. Rostamani, M.S. Bathaei, J. Manuf. Mater. Process. 6 (2022), doi:10.3390/jmmp6060158.
- [132] M. Esmaily, Z. Zeng, A.N. Mortazavi, A. Gullino, S. Choudhary, T. Derra, F. Benn, F. D'Elia, M. Mütther, S. Thomas, A. Huang, A. Allanore, A. Kopp, N. Birbilis, Addit. Manuf. 35 (2020) 101321, doi:10.1016/j.addma.2020.101321.
- [133] Z. Zhang, J. Shen, S. Hu, Y. Chen, C. Yin, X. Bu, Materials 16 (2023), doi:10.3390/ma16083236.
- [134] X. Yang, J. Liu, Z. Wang, X. Lin, F. Liu, W. Huang, E. Liang, Mater. Sci. Eng. A 774 (2020) 138942, doi:10.1016/j.msea.2020.138942.
- [135] X. Fang, J. Yang, S. Wang, C. Wang, K. Huang, H. Li, B. Lu, J. Mater. Process. Technol. 300 (2022) 117430, doi:10.1016/j.jmatprotec.2021.117430.
- [136] J. Li, Y. Qiu, J. Yang, Y. Sheng, Y. Yi, X. Zeng, L. Chen, F. Yin, J. Su, T. Zhang, X. Tong, B. Guo, J. Magnes. Alloy. 11 (2023) 217–229, doi:10.1016/j.jma.2021.04.007.
- [137] T. Ying, Z. Zhao, P. Yan, J. Wang, X. Zeng, Mater. Lett. 307 (2022) 131014, doi:10.1016/j.matlet.2021.131014.
- [138] Y. Guo, G. Quan, M. Celikin, L. Ren, Y. Zhan, L. Fan, H. Pan, J. Magnes. Alloy. 10 (2022) 1930–1940, doi:10.1016/j.jma.2021.04.006.
- [139] Y. Cao, Y. Zhang, W. Ming, W. He, J. Ma, Metals 13 (2023), doi:10.3390/met13020398.
- [140] C. Yin, J. Shen, S. Hu, Z. Zhang, Results Eng. 18 (2023) 101065, doi:10.1016/j.rineng.2023.101065.
- [141] H. Yi, Q. Wang, H. Cao, J. Mater. Res. Technol. 20 (2022) 627–649, doi:10.1016/j.jmrt.2022.07.083.
- [142] M. Ziaee, N.B. Crane, Addit. Manuf. 28 (2019) 781–801, doi:10.1016/j.addma.2019.05.031.
- [143] A. Mostafaei, E.L. Stevens, J.J. Ference, D.E. Schmidt, M. Chmielus, Addit. Manuf. 21 (2018) 63–68, doi:10.1016/j.addma.2018.02.014.
- [144] A. Mostafaei, A.M. Elliott, J.E. Barnes, F. Li, W. Tan, C.L. Cramer, P. Nandwana, M. Chmielus, Prog. Mater. Sci. 119 (2021) 100707, doi:10.1016/j.pmatsci.2020.100707.
- [145] C. Su, J. Wang, H. Li, Z. You, J. Li, J. Manuf. Process. 72 (2021) 71–79, doi:10.1016/j.jmapro.2021.09.061.
- [146] C. Su, J. Wang, H. Li, Z. You, J. Li, J. Manuf. Process. 84 (2022) 652–659, doi:10.1016/j.jmapro.2022.09.025.
- [147] F. Cao, Z. Shi, G.L. Song, M. Liu, M.S. Dargusch, A. Atrens, Corros. Sci. 94 (2015) 255–269, doi:10.1016/j.corsci.2015.02.002.
- [148] F. Khodabakhshi, A.P. Gerlich, J. Manuf. Process. 36 (2018) 77–92, doi:10.1016/j.jmapro.2018.09.030.
- [149] R.S. Mishra, R.S. Haridas, P. Agrawal, Sci. Technol. Weld. Join. 27 (2022) 141–165, doi:10.1080/13621718.2022.2027663.
- [150] W. Wang, P. Han, P. Peng, T. Zhang, Q. Liu, S.N. Yuan, L.Y. Huang, H.L. Yu, K. Qiao, K.S. Wang, Acta Metall. Sin. 33 (2020) 43–57, doi:10.1007/s40195-019-00971-7.
- [151] N. Afrin, D.L. Chen, X. Cao, M. Jahazi, Mater. Sci. Eng. A 472 (2008) 179–186, doi:10.1016/j.msea.2007.03.018.
- [152] S. Ghosh, C. Woodward, C. Przybyla, Integrated Computational Materials Engineering (ICME): Advancing Computational and Experimental Methods, Springer Nature, 2020.
- [153] M.F. Horstemeyer, Integrated Computational Materials Engineering (ICME) for Metals: Concepts and Case Studies, John Wiley & Sons, 2018.
- [154] N.R. Council, Integrated Computational Materials engineering: a Transformational Discipline for Improved Competitiveness and National Security, National Academies Press, 2008.
- [155] R. Shi, A.A. Luo, Calphad Comput. Coupling Phase Diagrams Thermochem. 62 (2018) 1–17, doi:10.1016/j.calphad.2018.04.009.
- [156] A.A. Luo, Calphad Comput. Coupling Phase Diagrams Thermochem. 50 (2015) 6–22, doi:10.1016/j.calphad.2015.04.002.
- [157] Z.K. Liu, J. Phase Equilibria Diffus. 30 (2009) 517–534, doi:10.1007/s11669-009-9570-6.
- [158] S. Ganeshan, S.L. Shang, Y. Wang, Z.K. Liu, Acta Mater. 57 (2009) 3876–3884, doi:10.1016/j.actamat.2009.04.038.
- [159] Y. Zhong, J.O. Sofo, A.A. Luo, Z.K. Liu, J. Alloys Compd. 421 (2006) 172–178, doi:10.1016/j.jallcom.2005.09.076.
- [160] H. Zhang, Y. Wang, S. Shang, L.Q. Chen, Z.K. Liu, J. Alloys Compd. 463 (2008) 294–301, doi:10.1016/j.jallcom.2007.09.020.
- [161] S.L. Shang, Y. Wang, Z.K. Liu, Magnes. Technol. (2010) 617–622.
- [162] W. Zhong, J.C. Zhao, Scr. Mater. 127 (2017) 92–96, doi:10.1016/j.scriptamat.2016.09.008.
- [163] B.C. Zhou, S.L. Shang, Y. Wang, Z.K. Liu, Acta Mater. 103 (2016) 573–586, doi:10.1016/j.actamat.2015.10.010.
- [164] W. Zhong, J.C. Zhao, Acta Mater. 201 (2020) 191–208, doi:10.1016/j.actamat.2020.09.079.
- [165] C. Zhang, J. Miao, S. Chen, F. Zhang, A.A. Luo, J. Phase Equilibria Diffus. 40 (2019) 495–507, doi:10.1007/s11669-019-00732-0.
- [166] G. Han, Z. Han, A.A. Luo, B. Liu, Metall. Mater. Trans. A Phys. Metall. Mater. Sci. 46 (2015) 948–962, doi:10.1007/s11661-014-2674-6.
- [167] G. Han, Z. Han, A.A. Luo, A.K. Sachdev, B. Liu, Scr. Mater. 68 (2013) 691–694, doi:10.1016/j.scriptamat.2013.01.018.
- [168] R.W. Cahn, Int. J. Mater. Res. 84 (1993) 573.
- [169] J. Zhang, E. Cinkilic, X. Huang, G.G. Wang, Y. (Chad) Liu, J.P. Weiler, A.A. Luo, Mater. Sci. Eng. A 865 (2023) 144604, doi:10.1016/j.msea.2023.144604.
- [170] C. Zhang, W. Cao, S.L. Chen, J. Zhu, F. Zhang, A.A. Luo, R. Schmid-Fetzer, JOM 66 (2014) 389–396, doi:10.1007/s11837-014-0879-1.
- [171] X. Xia, W. Sun, A.A. Luo, D.S. Stone, Acta Mater. 111 (2016) 335–347, doi:10.1016/j.actamat.2016.03.068.
- [172] J. Miao, C. Zhang, A.D. Klarner, J. Zhang, E. Cinkilic, F. Zhang, A.A. Luo, Materialia 21 (2022) 101348, doi:10.1016/J.MTLA.2022.101348.
- [173] A. Atrens, X. Chen, Z. Shi, Corros. Mater. Degrad. 3 (2022) 566–597, doi:10.3390/cmd3040031.
- [174] Y. Yang, X. Xiong, J. Chen, X. Peng, D. Chen, F. Pan, J. Magnes. Alloy. 9 (2021) 705–747, doi:10.1016/j.jma.2021.04.001.
- [175] S. Thomas, N.V. Medhekar, G.S. Frankel, N. Birbilis, Curr. Opin. Solid State Mater. Sci. 19 (2015) 85–94, doi:10.1016/j.cossms.2014.09.005.
- [176] L.J. Liu, M. Schlesinger, Corros. Sci. 51 (2009) 1733–1737, doi:10.1016/j.corsci.2009.04.025.
- [177] G. Song, A. Atrens, Adv. Eng. Mater. 5 (2003) 837–858, doi:10.1002/adem.200310405.
- [178] A. Atrens, W. Dietzel, Adv. Eng. Mater. 9 (2007) 292–297, doi:10.1002/adem.200600275.
- [179] G. Song, A. Atrens, D. St. John, X. Wu, J. Nairn, Corros. Sci. 39 (1997) 1981–2004, doi:10.1016/S0010-938X(97)00090-5.
- [180] G. Song, A. Atrens, D. Stjohn, J. Nairn, Y. Li, Corros. Sci. 39 (1997) 855–875.
- [181] G.S. Frankel, A. Samaniego, N. Birbilis, Corros. Sci. 70 (2013) 104–111, doi:10.1016/j.corsci.2013.01.017.
- [182] J. Huang, G.L. Song, A. Atrens, M. Dargusch, J. Mater. Sci. Technol. 57 (2020) 204–220, doi:10.1016/j.jmst.2020.03.060.
- [183] R.M. Fogarty, A.P. Horsfield, J. Chem. Phys. 157 (2022), doi:10.1063/5.0105828.
- [184] T. Würger, C. Feiler, G.B. Vonbun-Feldbauer, M.L. Zheludkevich, R.H. Meißner, Sci. Rep. 10 (2020) 1–11, doi:10.1038/s41598-020-71694-4.
- [185] J. Huang, G.L. Song, Y. Zhu, D. Zheng, Z. Wang, J. Magnes. Alloy. 11 (2023) 230–248, doi:10.1016/j.jma.2021.05.008.
- [186] A.S. Gnedenkov, S.L. Sinebryukhov, V.S. Filonina, V.S. Egorin, A.Y. Ustinov, V.I. Sergienko, S.V. Gnedenkov, J. Magnes. Alloy. 10 (2022) 1326–1350, doi:10.1016/j.jma.2021.11.027.
- [187] K. Kondoh, R. Takei, S. Kariya, S. Li, J. Umeda, Mater. Lett. 319 (2022) 132266, doi:10.1016/j.matlet.2022.132266.
- [188] C. Xu, J. Wang, C. Chen, C. Wang, Y. Sun, S. Zhu, S. Guan, J. Magnes. Alloy. 11 (2021) 958–965, doi:10.1016/j.jma.2021.06.017.

- [189] A. Atrens, Z. Shi, S.U. Mehreen, S. Johnston, G.L. Song, X. Chen, F. Pan, J. Magnes. Alloy. 8 (2020) 989–998, doi:10.1016/j.jma.2020.08.002.
- [190] Q. Zhu, Y. Li, F. Cao, D. Qiu, Y. Yang, J. Wang, H. Zhang, T. Ying, W. Ding, X. Zeng, Nat. Commun. 13 (2022), doi:10.1038/s41467-022-33480-w.
- [191] J.D. Hanawalt, C.E. Nelson, J.A. Peloubet, Trans. Am. Inst. Mining, Metall. Pet. Eng. 147 (1942) 273–299.
- [192] J.E. Hillis, SAE Tech. Pap. 92 (1983) 553–559, doi:10.4271/830523.
- [193] Y. Zhang, Y. Huang, X. Chen, B. Luthringer-Feyerabend, J. Xue, D. Zander, R. Willumeit-Römer, K.U. Kainer, N. Hort, Scr. Mater. 212 (2022) 114509, doi:10.1016/j.scriptamat.2022.114509.
- [194] L. Yang, G. Liu, L. Ma, E. Zhang, X. Zhou, G. Thompson, Corros. Sci. 139 (2018) 421–429, doi:10.1016/j.corsci.2018.04.024.
- [195] A. Pardo, M.C. Merino, A.E. Coy, R. Arrabal, F. Viejo, E. Matykina, Corros. Sci. 50 (2008) 823–834, doi:10.1016/j.corsci.2007.11.005.
- [196] S.K. Woo, B.C. Suh, H.S. Kim, C.D. Yim, Corros. Sci. 184 (2021) 109357, doi:10.1016/j.corsci.2021.109357.
- [197] M. Liu, P.J. Uggowitzer, P. Schmutz, A. Atrens, JOM 60 (2008) 39–44, doi:10.1007/s11837-008-0164-2.
- [198] M. Liu, P.J. Uggowitzer, A.V. Nagasekhar, P. Schmutz, M. Easton, G.L. Song, A. Atrens, Corros. Sci. 51 (2009) 602–619, doi:10.1016/j.corsci.2008.12.015.
- [199] J. Hofstetter, E. Martinelli, A.M. Weinberg, M. Becker, B. Mingler, P.J. Uggowitzer, J.F. Löffler, Corros. Sci. 91 (2015) 29–36, doi:10.1016/j.corsci.2014.09.008.
- [200] M. Deng, L. Wang, D. Snihirova, J. Bohlen, G. Kurz, S.V. Lamaka, D. Höche, M.L. Zheludkevich, J. Magnes. Alloy. 11 (2023) 1193–1205, doi:10.1016/j.jma.2022.12.014.
- [201] H. Ibrahim, A.D. Klarner, B. Poorganji, D. Dean, A.A. Luo, M. Elahinia, J. Mech. Behav. Biomed. Mater. 69 (2017) 203–212, doi:10.1016/j.jmbbm.2017.01.005.
- [202] L. Yang, X. Zhou, S.M. Liang, R. Schmid-Fetzer, Z. Fan, G. Scamans, J. Robson, G. Thompson, J. Alloys Compd. 619 (2015) 396–400, doi:10.1016/j.jallcom.2014.09.040.
- [203] M. Deng, L. Wang, D. Höche, S.V. Lamaka, C. Wang, D. Snihirova, Y. Jin, Y. Zhang, M.L. Zheludkevich, Mater. Horizons 8 (2021) 589–596, doi:10.1039/d0mh01380c.
- [204] K. Zhang, C. Wang, D.W. Wang, M.X. Li, Y.L. Ma, Z.M. Hua, L.Y. Zhang, J. Li, H.Y. Wang, Corros. Sci. 213 (2023) 110971, doi:10.1016/j.corsci.2023.110971.
- [205] J. Yang, J. Peng, E.A. Nyberg, F.S. Pan, Appl. Surf. Sci. 369 (2016) 92–100, doi:10.1016/j.apsusc.2016.01.283.
- [206] W.C. Kim, J.G. Kim, J.Y. Lee, H.K. Seok, Mater. Lett. 62 (2008) 4146–4148, doi:10.1016/j.matlet.2008.06.028.
- [207] R.C. Zeng, W.C. Qi, H.Z. Cui, F. Zhang, S.Q. Li, E.H. Han, Corros. Sci. 96 (2015) 23–31, doi:10.1016/j.corsci.2015.03.018.
- [208] H.R.B. Rad, M.H. Idris, M.R.A. Kadir, S. Farahany, Mater. Des. 33 (2012) 88–97, doi:10.1016/j.matdes.2011.06.057.
- [209] X.B. Chen, N.T. Kirkland, H. Krebs, M.A. Thiriat, S. Virtanen, D. Nisbet, N. Birbilis, Corros. Eng. Sci. Technol. 47 (2012) 365–373, doi:10.1179/1743278212Y.0000000019.
- [210] S.E. Harandi, M. Mirshahi, S. Koleini, M.H. Idris, H. Jafari, M.R.A. Kadir, Mater. Res. 16 (2013) 11–18, doi:10.1590/S1516-14392012005000151.
- [211] T. Takenaka, T. Ono, Y. Narazaki, Y. Naka, M. Kawakami, Electrochim. Acta. 53 (2007) 117–121, doi:10.1016/j.electacta.2007.03.027.
- [212] Y. Song, D. Shan, E.H. Han, J. Mater. Sci. Technol. 33 (2017) 954–960, doi:10.1016/j.jmst.2017.01.014.
- [213] J. Liu, Y. Song, J. Chen, P. Chen, D. Shan, E.H. Han, Electrochim. Acta. 189 (2016) 190–195, doi:10.1016/j.electacta.2015.12.075.
- [214] R. Pinto, M.G.S. Ferreira, M.J. Carmezim, M.F. Montemor, Electrochim. Acta. 56 (2011) 1535–1545, doi:10.1016/j.electacta.2010.09.081.
- [215] R.D.K. Misra, Mater. Lett. 331 (2023) 133443, doi:10.1016/j.matlet.2022.133443.
- [216] Z. Savaedi, H. Mirzadeh, R.M. Aghdam, R. Mahmudi, Mater. Today Commun. 33 (2022) 104825, doi:10.1016/j.mtcomm.2022.104825.